HHS Public Access

Author manuscript

ACS Appl Mater Interfaces. Author manuscript; available in PMC 2019 January 18.

Published in final edited form as:

ACS Appl Mater Interfaces. 2018 May 30; 10(21): 17792–17808. doi:10.1021/acsami.8b05607.

pH-Sensitive Multi-ligand Gold Nanoplatform Targeting Carbonic Anhydrase IX Enhances the Delivery of Doxorubicin to Hypoxic Tumor Spheroids and Overcomes the Hypoxia-Induced Chemoresistance

Ahmed M. Shabana[1], **Utpal K. Monda**[1], **Md. Raqibul Alam**[1], **Taylor Spoon**[2], **Codee Alicia Ross**[2], **Muniswamy Madesh**[3], **Claudiu T. Supuran**[4], and **Marc A. Ilies**[1,*]

[1]Department of Pharmaceutical Sciences and Moulder Center of Drug Discovery Research, Temple University School of Pharmacy, 3307 N Broad Street, Philadelphia, PA-19140

[2]College of Science and Technology, Temple University, 1803 N Broad Street, Philadelphia, PA-19122

[3]Department of Biochemistry, Temple University School of Medicine, 3500 N Broad Street, Philadelphia, PA-19140, USA

[4]NEUROFARBA Department, Pharmaceutical Sciences Section, Universita degli Studi di Firenze, Polo Scientifico, Via Ugo Schiff no. 6, 50019 Sesto Fiorentino (Florence), Italy

Abstract

Hypoxia is a common feature of solid tumors contributing to resistance to chemotherapy. Selective delivery of chemotherapeutic drugs to hypoxic tumor niche remains an unsolved issue. For this purpose, we constructed a gold nanoplatform targeting carbonic anhydrase IX (CA IX) epitope, which is overexpressed in hypoxic tumor cells versus normal tissues. We designed compatible small MW carbonic anhydrase inhibitor ligands (CAI)- and doxorubicin (Dox)-ligands, and optimized protocols for AuNPs efficient decoration to achieve both good targeting ligand density and optimum drug loading, while preserving colloidal stability. The optimized Dox-HZN-DTDP @ Au NPs-LA-PEG2000-CAI (THZN) nanoplatform proved to be very efficient towards killing HT-29 tumor cells, especially under hypoxic conditions as compared to the non-targeted nanoplatform. It also mediated the effective release of doxorubicin in the lysosomes following internalization, as revealed by confocal microscopy. Furthermore, using tumor spheroids as a representative model for hypoxic solid tumors, our THZN nanoplatform enhanced up to 2.5 times the selective delivery of doxorubicin and minimized chemoresistance, showing better tumor drug penetration as compared to free drug treatment. Our technology is the first CA IX-targeted gold

*To whom correspondence should be addressed Tel 215-707-1749, Fax 215-707-5620, mailies@temple.edu (MAI).

Conflicts of interest

There are no conflicts of interest to declare

Supporting Information

The supporting information is available free of charge on the ACS Publication website at DOI: Preparation of CAI- and Dox- ligands and conjugates, characterization of citrate-stabilized gold nanoparticles, CA inhibition assay of functionalized gold nanoplatforms, preparation of gold nanoplatforms, determination of doxorubicin content of doxorubicin loaded Au nanoplatforms, release of doxorubicin from the Au nanoplatforms as a function of pH.

nanoplatform for efficient delivery of doxorubicin to hypoxic tumors in a controlled fashion, with the perspective to improve the therapy of solid tumors and minimize chemoresistance.

Keywords

gold nanoparticles; hypoxia; carbonic anhydrase IX; inhibitor; doxorubicin delivery; tumor spheroids; chemoresistance

Introduction

Gold nanoparticles (Au NPs) have emerged as a robust and versatile platform technology for diagnostic and delivery purposes during recent years, due to their unique physicochemical and optical properties and excellent biocompatibility.[1–5] Examples of biological applications include delivery of enzyme inhibitors,[6] activators,[7] various drugs,[8–9] oligonucleotides[10] and nucleic acids. [4, 11] Au NPs can be reliably manufactured under a variety of shapes and sizes and can be decorated with a plethora of ligands to achieve the functional nanoplatforms desired. [1–4, 12] Using ligands strategically designed against epitopes expressed on cells in pathological states, as well as various drug conjugates, Au NPs can function as targeted delivery systems in the detection and treatment of various dysfunctions and diseases, including cancer. [9, 13–14] Focusing on cancer treatment, it must be emphasized that solid tumors are particularly difficult to treat, due to their plastic metabolism, fast mutation rate and hypoxic nature, which make them resistant to many chemotherapeutic agents.[15–16]

On the other hand, over the last decade a connection was established between hypoxic tumors and the expression of certain isozymes of carbonic anhydrase, (CA) a ubiquitous zinc metalloenzyme that catalyzes the reversible hydration of carbon dioxide to bicarbonate ($CO_2 + H_2O \rightleftharpoons HCO_3^- + H^+$). Through its fifteen CA isozymes with different catalytic activity, subcellular localization, and tissue distribution described to date in humans, CA plays a critical role in cellular respiration and CO2 transport between metabolizing tissues and lungs, pH and CO2 homeostasis, electrolyte and aqueous humor secretion, biosynthetic reactions, etc.[17–18] Recent studies have shown that many fast growing solid tumors become hypoxic and that hypoxia triggers the expression of hundreds of genes, including carbonic anhydrase IX.[17–19] Thus, CA IX is over-expressed in many tumor cells, and was associated with poor prognosis in breast, colorectal, ovarian, bladder, head and neck, cervical, brain, pancreatic and renal cancer, [17–19] etc. Thus, hypoxia was shown to enhance tumor resistance to chemo- and radiotherapy.[20] CA IX normal expression in the human body is restricted to the epithelium of stomach, duodenum and upper small intestine, which makes it a particularly appealing epitope to target by anticancer delivery systems.[17, 21]

Importantly, CA IX is a dimeric membrane-bound CA isozyme, attached on the outer surface of plasma membrane, where it regulates the extracellular pH and CO2/$HCO3^-$ pools. [17, 19, 21]Its role becomes critical in hypoxic tumors, where glycolysis is upregulated to supply the fast dividing cancer cells with ATP and cellular building blocks (Warburg effect). [16, 23] Here, CA IX works in tandem with cytosolic isozymes, especially CA II, to facilitate the efficient transport of glycolytic protons from cytoplasm to exterior of the cell.[17, 19, 21]

Acidification of external milieu prevents the access of basic chemotherapeutic drugs to the tumor, contributing to tumor resistance to chemotherapy.[24]

Inhibition of CA IX was exploited for detection, imaging and killing of hypoxic solid tumors.[17, 19, 25–26] The CA IX active site(s) share a high structural homology to other CA isozymes, all being efficiently inhibited by (unselective) classical CA inhibitors such as aromatic and heterocyclic sulfonamides, and their sulfamide and sulfamates isosteres.[17–18, 26–28] Despite this fact, our team has shown that it is possible to obtain selective inhibitors for membrane CA isozymes, including CA IX, by making the CA inhibitors membrane-impermeant, either through attached charged moieties[29–30] or via oligoethyleneglycol (oligoEG)- and polyethyleneglycol (PEG) conjugation.[25] Notably, both oligoEG- and PEGylated CA IX inhibitors proved able to control the growth of several hypoxic carcinomas over-expressing CA IX.[25]

Building on these studies, we are translating our oligoEG- and PEGylated CAI conjugates into efficient targeting ligands for gold nanoparticles to focus their delivery to hypoxic tumor cells and to promote tumor killing. Furthermore, we used PEGylated CA IX targeted AuNPs to deliver chemotherapeutic agent doxorubicin (Dox), in a novel multi-ligand Au nanoplatform designed to selectively release the drug intracellularly, in order to enhance the selective tumor drug uptake and killing.

Materials and Methods

Materials

The following materials were used as received: succinic anhydride (TCI America, Portland, OR), 2,2`-(ethylenedioxy)-diethylamine (Fluka, St Louis, MO), N-methylmorpholine (TCI America, Portland, OR), 2-chloro-4,6-dimethoxy-1,3,5-triazine (Acros Organics, New Jersey, NJ), H2N-PEG2000-NH2 and H2N-PEG2000-OCH3 (Laysan Bio, Arab, AL). Other solvents (HPLC quality) were purchased from Fisher Scientific (Pittsburgh, PA), EMD (Gibbstown, NJ), and VWR International (West Chester, PA). Sodium citrate dihydrate, was from Sigma-Aldrich, HAuCl4 trihydrate was from LabChem Inc, Hydrochloric acid 37% and nitric acid 68% were from BDH chemicals, lipoic acid from Alfa Aesar, thiazolyl blue tetrazolium bromide (MTT) from Affymetrix, hydrazine hydrate from Acros Organics, RIPA lysis buffer and NaOH were purchased from Amresco, doxorubicin hydrochloride from TRC Canada, dithiodipropionic acid from Aldrich.

Techniques

The purity and structure identity of the intermediary and the final products were assessed by a combination of techniques that included thin-layer chromatography (TLC), HPLC-MS, ^{1}H-NMR, COSY, ^{13}C-NMR, HRMS and MALDI. TLC was carried out on SiO2-precoated aluminum plates (silica gel with F254 indicator; layer thickness 200 μm; pore size 60 Å, from Sigma-Aldrich.

Melting points were determined using a Thermolyne heating stage microscope (Dubuque, IA), equipped with an Olympus 5X objective, at heating/cooling rate of ~ 4 ^{o}C/min and were uncorrected.

The purity of compounds was assessed via LC-MS using an Agilent 1200 HPLC-DAD-MS system equipped with a G1315A DAD and a 6130 Quadrupole MS using ZORBAX SB-C18 column, eluted with H2O (0.1% HCOOH)/MeCN (0.1% HCOOH) 95/5 to 0/100 linear gradient.

NMR spectra were recorded at ≈300 K with a Bruker Avance III 400 Plus spectrometer equipped with a 5 mm indirect detection probe, operating at 400 MHz for ^{1}H-NMR, at 100 MHz for ^{13}C-NMR. Chemical shifts are reported as δ values, using tetramethylsilane (TMS) as internal standard for proton spectra and the solvent resonance for carbon spectra. Assignments were made based on chemical shifts, signal intensity and COSY sequences. For ^{1}H-NMR, data are reported as follows: chemical shift, multiplicity (s = singlet, d = doublet, t = triplet, sep = septet, m = multiplet), coupling constants J (Hz) and integration.

High resolution mass spectrometry (HR-MS) was performed on a LTQ Orbitrap XL hybrid ion trap-orbitrap mass spectrometer (Thermo Scientific, Waltham, MA).

Analytical GPC was performed for the polymeric compounds using a Shimadzu prominence UFLC equipped with vacuum degasser, CC20AD pump, CBM 20A controller, CTO – 20 A column over, UV and RI detectors, under the control of EZ start software. Separation was performed with Phenomenex Phenogel columns (1 × Phenogel Guard column, 5μ, linear, 50 × 7.8 mm + 1 × Phenogel 5μ, 100 Å, 300 × 7.8 mm + 1 × Phenogel 5μ, 500 Å, 300 × 7.8 mm) eluted with DMF, at 50°C, at a flow rate of 1 mL/min. Calibration was done with 10 PEG standards, ranging from 200 to 5000 MW. MALDI-TOF was performed on a Bruker Daltonix Autoflex TOF-TOF mass spectrometer, using α-cyano-4-hydroxycinnamic acid as matrix. Samples were dissolved in MeCN containing 0.1% TFA at a concentration of 1 mg/mL. Equal volumes of sample and matrix (5 mg/mL in MeCN) were mixed and the solution was spotted on the MALDI plate. After drying, the plate was inserted into the instrument and the spectrum was determined, using a 20000V acceleration voltage and a variable bombardment time.

The starting aminosulfonamide 5-amino-1,3,4-thiadiazole-2-sulfonamide **2** was synthesized as described previously.[25–26] The synthesis and characterization of CAI ligands and Dox ligands is presented in the Supporting Information.

Synthesis of citrate stabilized gold nanoparticles

Gold nanoparticles were prepared using Turkevich method. [31] All glassware used in the preparation was cleaned with Aqua Regia (3 parts conc. HCl and 1 part conc. HNO3) then rinsed three times with deionized water and dried in the oven. A volume of 25 mL of 1 mM HAuCl4 stock solution was diluted to 50 mL with deionized water in a 100 mL rounded bottom flask. The flask was heated to boiling using an oil bath under vigorous stirring and 750 μL of 38.8 mM sodium citrate was added. The solution was stirred while boiling for 10 min, after which heating was stopped and stirring was continued for another 10 min. The resulting citrate capped gold nanoparticle colloidal solution was filtered through a 0.22 μm membrane filter. Excess citrate was removed by centrifuging the colloidal solution at 10000 rpm for 15 min, removing the supernatant and resuspending the gold nanoparticles in water with pH adjusted to 10 using 0.1 M NaOH. The size and zeta potential of the nanoparticles

were monitored throughout the process. The concentration of the gold nanoparticles was determined via inductively coupled plasma optical emission spectroscopy (ICP-OES) using a calibration curve made with standards of known gold concentration.[32]

Functionalization of gold nanoparticles with various CAIs thiolated ligands

Ligands stock solutions were prepared at a concentration of 0.02 M in absolute ethanol. For functionalization, 100 μL of prepared citrate capped nanoparticles were treated with predetermined volume (30 μL) of stock solutions of lipoic acid (LA), lipoic acid-CAI (LA-CAI), lipoic acid- PEG2000 (LA-PEG2000) and lipoic acid-PEG2000-CAI (LA-PEG2000-CAI). All samples were sonicated for 5 min using a bath sonicator then allowed to rest in the dark for 24 h. The next day all samples were filtered through 0.22 μm membrane filter and excess ligand was removed by centrifuging the samples at 10000 rpm for 15 min, removing the supernatant, and resuspending the functionalized Au NPs in DI water. Cleaning was repeated once, to leave the Au NPs into a final volume of 100 μL DI water. The concentration of the functionalized gold nanoparticles was determined via ICP-OES using a calibration curve made with standards of known gold concentration.

Characterization of citrate capped and functionalized gold nanoparticles

The size and the zeta potential of the Au NPs were determined via a Zetasizer Nano ZS (Malvern Instruments, Malvern, UK) using a disposable Malvern DTS 1060 measurement cell. The plasmon spectra of nanoparticles was recorded using a Spectramax M2 UV-Vis spectrophotometer in the range of 400–850 nm. A refractive index of 0.200 and a max absorbance of 3.320 were used for gold nanoparticles size measurement. The shape and morphology of the gold nanoparticles were examined via transmission electron microscope (TEM), which was performed on a JEOL JEM1400 EM with an operating voltage of 80 KeV. A drop of various samples was placed on type-A 300 mesh copper TEM grids (Ted Pella, Inc., Redding, CA), and the grids were air-dried for 10–15 min, then placed in a vacuum chamber. Images were captured using a Gatan Outer SCAN 1000 CCD Camera. Image capture, processing, and analysis were performed with Gatan Digital Micrograph software. The concentration of the generated gold nanoparticles was determined using inductively coupled plasma optical emission spectroscopy (ICP-OES) using a calibration curve made with standards of known gold concentration.

Carbonic anhydrase inhibition assay

The carbonic anhydrase (CA) inhibition potential of different Au NPs preparation was assessed by incubating 25 μM of Au NPs, Au NPs-LA, Au NPs-LA-CAI, Au NPs-LA-PEG2000 and Au NPs-LA-PEG2000-CAI with stock solution of CA II isozyme (1 mg/ml) prepared in HBS buffer. The esterase activity of CA II was assessed by adding 100 μL of p-nitrophenylacetate, which is converted to p-nitrophenol. The absorbance of the solution at 400 nm was measured at different time intervals. The inhibition ability of Au NPs formulation was compared to the inhibition performed by acetazolamide, a known potent CA inhibitor. Similarly, CA II isozyme was incubated with 1, 2.5 and 5 μM acetazolamide in the presence of 25 μM citrate capped gold nanoparticles, followed by addition of 100 μL of 0.01 M paranitrophenyl acetate. Absorbance was recorded at 400 nm at different time intervals.

Cell culture studies

HT-29 colorectal cancer cell line (ATCC-HTB-38) was used in this study. Cells were allowed to grow in RPMI-1640 medium containing 10 % FBS and sub cultured periodically in T-75 culture flasks, maintained in a humidified atmosphere containing 5% CO2, at 37 ^{O}C. Media was changed every other day.

Validation of CA IX expression in HT-29 cells under hypoxic conditions by western blotting

HT-29 cell line was examined for expression of CA IX in 2D culture under both normoxic and hypoxic conditions. Cells were cultured in 60 mm Petri dishes at a density of 10^6 cells/dish and maintained under normoxic conditions. Hypoxia was generated by placing half of the dishes in a hypoxic chamber purged with hypoxia gas mixture containing 1% O2, 5% CO2 and 94% N2 for 24 h. The next day, media was removed, cells were washed with PBS, harvested, pelleted, subsequently lysed with RIPA buffer containing protease inhibitors, and lysates were collected and stored at −20 °C. Total protein concentration was determined using bicinchoninic acid (BCA) assay (Thermo Scientific, Rockford, IL). Western Blot analysis was performed as described.[25] Briefly, cell lysate samples were loaded onto 10% SDS-PAGE precast gels (Biorad, Cat. 456–8034), and protein separation was done at 150 V for 2 h. Gels were transblotted onto nitrocellulose membranes for 30 min, and membranes were blocked using blocking buffer (Odyssey blocking buffer from Licor Cat. 927–40000) followed by incubation with a specific primary mouse monoclonal antibody for CA IX (M75, Bioscience Slovakia) at 4 °C overnight. After washing, membranes were incubated with antimouse IgG IRDye800CW secondary antibody (Rockland) for 1 h at room temperature. Finally, membranes were detected using an Odyssey image system (Li-Cor, Lincoln NE). Beta actin was used as a control and was detected using a mouse monoclonal beta actin antibody (Genetex) followed by detection with the same IgG IRDye800CW secondary antibody.

Uptake of functionalized Au NPs under normoxic and hypoxic conditions using ICP-OES

The cell uptake of Au NPs was investigated quantitatively by inductively coupled plasma optical emission spectroscopy (ICP-OES). Cells were seeded into 6 well plates at density of 5×10^5 cells/well. The next day, one plate was placed into a hypoxic chamber purged with hypoxia gas mixture containing 1 % O2, 5% CO2 and 94% N2 and hypoxic conditions were maintained for 24 h. The other plate was kept under normoxic conditions at 37 ^{O}C and 5% CO2. After 24 h, cells were washed with PBS and treated Au NPs-LA, Au NPs-LA -CAI, Au NPs LA-PEG2000 and Au NPs- LA-PEG2000-CAI nanoparticles diluted in media at 50 μM concentration for 24 h incubation period. After Au NPs treatment, media was aspirated and cells were washed twice with PBS, trypsinized with 1 mL trypsin-EDTA and transferred into 15 mL falcon tubes. Cells were pelleted through centrifugation at 3000 rpm for 5 min, then supernatant was removed and cells were resuspended in 1 mL aqua regia for 24 h. The final samples were diluted to 5 mL final volume with deionized water and analyzed by ICP-OES. A standard curve was constructed using gold stock solutions of known concentrations. Results are expressed as average ± one standard deviation.

Uptake of functionalized Au NPs by HT-29 cancer cells using silver staining

HT-29 cancer cells were seeded into 6 well plates at density of 5×10^5 cells/well. The next day, one plate was placed into a hypoxic chamber purged with hypoxia gas mixture containing 1 % O2, 5% CO2 and 94% N2 and hypoxic conditions were maintained for 24 h. The other plate was kept under normoxic conditions at 37 ^{O}C and 5% CO2. After 24 h, cells were washed with PBS and treated Au NPs-LA, Au NPs-LA -CAI, Au NPs LA-PEG2000 and Au NPs- LA-PEG2000-CAI nanoparticles diluted in media at 50 μM concentration for 24 h incubation period. Cells treated with only media served as a control. After Au NPs treatment, media was aspirated and cells were washed twice with PBS and fixed with 4% paraformaldehyde followed by addition of equal volumes of silver benzoate and hydroquinone (prepared in citrate buffer pH 3.8) for 15 min. Following incubation period, cells were quickly washed with water and then examined under confocal microscope and images were acquired in bright field mode.

Viability assay to determine the cytotoxicity of citrate capped and functionalized gold nanoparticles.

The cytotoxicity of various gold nanoparticles preparations was conducted using MTT assay. HT-29 cells were seeded into two 96 well plates at a density of 20,000 cells/well and were allowed to attach for 24 h. The next day one plate was placed into a hypoxic chamber purged with hypoxia gas mixture containing 1 % O2, 5% CO2 and 94% N2 and hypoxic conditions were maintained for 24 h. The other plate was kept under normoxic conditions at 37 ^{O}C and 5% CO2. After 24 h, cells were washed with PBS and treated with different gold nanoparticles preparations diluted in media at three different concentrations (25 μM, 50 μM, and 100 μM) for 24 h. After Au NPs treatment, media was aspirated and cells were washed twice with PBS and treated with 120 μL of MTT solution (5 mg/mL) in media for 4 h. The MTT solution was aspirated and 150 μL of DMSO was added to each well to lyse the cells and solubilize the formed blue formazan crystals. The amount of formazan was evaluated spectrophotometrically at 570 nm with a reference absorbance at 690 nm. Each experiment was done in quadruplicate. A control experiment was done in parallel in which cells received just media without Au NPs. Viability is expressed as a percentage of control and data is expressed as average ± one standard deviation.

Gold nanoparticles functionalization strategies with Dox ligands and determination of doxorubicin content of resulting nanoplatforms. Detailed procedures are provided in the Supporting Information, sections S4-S9.

Cytotoxicity (MTT) assay of Doxorubicin loaded CA IX targeted gold nanoparticles

The cytotoxicity of free doxorubicin, Au NPs-LA-PEG2000, Au NPs-LA-PEG2000-CAI, and doxorubicin loaded DOX-AM-DTDP @ Au NPs-LA-PEG2000 (NTAM), DOX-HZN-DTDP @ Au NPs-LA-PEG2000 (NTHZN) and doxorubicin loaded CAI targeted Au NPs, DOX-AM-DTDP @ Au NPs-LA-PEG2000 (TAM), DOX-HZN-DTDP @ Au NPs-LA-PEG2000 (THZN) were determined using MTT assay. Two 96 well plates were seeded with HT-29 cells at a density of 20,000 cells/well and cells were allowed to attach for 24 h. The next day one plate was placed into a hypoxic chamber purged with hypoxia gas mixture containing 1 % O2, 5% CO2 and 94% N2 and hypoxic conditions was maintained for 24 h.

The other plate was kept under normoxic conditions at 37 ^{O}C and 5% CO2. After 24 h, the pH of cells was checked with a pH meter and found to be 7.14 for normoxic cells and 6.84 for hypoxic cells. Cells were washed with PBS and treated with different gold nanoparticles preparations having Au NPs at a nominal concentration of 100 μM (confirmed by ICP) on media for 48 h. The total amount of doxorubicin loaded onto Au NPs-LA-PEG2000 cleavable and Au NPs-LA-PEG2000-CAI cleavable, assessed by fluorescence as presented above, was 2.16 μg/ml and 2.27 μg/ml respectively. Based on these estimates the concentration of free doxorubicin used in the doxorubicin control wells was set at 4 μM (2.3 μg/ml). After treatment, media was aspirated and cells were washed twice with PBS and treated with 120 μL of MTT solution (5 mg/mL) in media for 4 h. The MTT solution was aspirated and 150 μL of DMSO was added to each well to lyse the cells and solubilize the formed blue formazan crystals. The amount of formazan was evaluated spectrophotometrically at 570 nm with a reference absorbance at 690 nm. Each experiment was done in quadruplicate. A control experiment was done in parallel for each plate, in which cells received just media. Viability was expressed as a percentage of control and data was expressed as average ± one standard deviation.

Intracellular tracking of Dox loaded Au NPs via confocal microscopy

HT-29 cells were cultured as described above. A total number of 1×10^6 cells were harvested, pelleted into 250 μL media and mixed with 20 μL of Rab-7-GFP plasmid 1 mg/mL in water and 2 μL of 10 × sterile PBS to ensure an isotonic solution. The suspension was transferred to a 0.4 cm Gene Pulser cuvette (Bio-Rad, Hercules, CA) and electroporated once at 200 mV and 960 μF and infinite resistance using a Bio-Rad MicroPulser electroporator (Bio-Rad, Hercules, CA). The cells were transferred into a sterile Falcon tube with 10 mL of media containing 10% FBS, allowed to recover for 3 h at 37^{O}C, and then plated at a density of 1×10^5 on glass coverslips in 6-well plates. The next day, the cells were introduced into a hypoxic chamber purged with hypoxia gas mixture containing 1% oxygen, 5% CO2, 94% N2 for 24 h. The cells were then treated for 4 h and 24 h with Dox-HZN-DTDP @ Au NPs-LA-PEG2000 (NTHZN) and Dox-HZN-DTDP @ Au NPs-LA-PEG2000-CAI (THZN), with both preparation having a Dox concentration of 1 μg/ml. After the treatment period, the coverslips were fished out, washed with PBS, then imaged for Rab-7-GFP expression (Exc. 488 nm) and Dox (Exc. 561 nm) via laser scanning confocal fluorescence microscopy using a Carl Zeiss 510 fluorescent microscope.

Delivery of doxorubicin into HT-29 tumor spheroids via gold nanoplatforms and comparison with free drug administration

Tumor spheroids were generated as previously described.[33] Briefly, HT-29 cancer cells were seeded at a density of 1000 cells/well in a rounded bottom 96 well plates (Lipidure A-U96 plates, NOF, Tokyo, Japan) using RPMI-1640 media supplemented with 10 % FBS at 37 ^{O}C to initiate the growth of the spheroids. The growth pattern of the spheroid was monitored for 10 days. At day 10, spheroids were treated with either free doxorubicin (5 μg/mL), or with NTHZN and THZN gold nanoplatforms containing the same doxorubicin concentration for 1 h treatment period. The amount of doxorubicin delivered into the tumor spheroids was

visualized by confocal fluorescence microscopy and quantified by fluorescence spectroscopy.

In the first method, the spheroids were then fished out onto a 35 mm petri dish and washed with PBS, then imaged through laser-scanning confocal flurosecence microscopy using a CARL Zeiss 710 fluorescent microscope at 488 nm excitation wavlength. Z-stack images were aquired at 40 μm interval and data was processed using the ZEN 2011 software.

In the second method, the spheroids were then fished out into 1.5 mL eppendorf tubes and gently pelleted down (5000 rpm for 5 min). Supernantant was discarded and spheroids were resuspended into PBS. The PBS washing procedure was repeated twice then the spheroids were pelleted down then lysed using cell lysis buffer (50 μL) for 1 h, using sonication. Quantification of doxorubicin was done by fluroscence spectroscopy, using an excitation wavelength of 488 nm and an emission wavelength of 570 nm, against a calibration curve constructed with known amounts of drug. A bicinchoninic protein assay was run in parallel to determine the amount of protein in each sample[33] and the amount of drug (in ng) was normalized for total protein. The results were expressed as amount of doxorubicin delivered (ng) per microgram of tumor spheroid protein.

Results and Discussion

Targeting ligand synthesis.

Very small (3–4 nm) gold nanoparticles decorated with short CAI inhibitors were shown by one of us to efficiently inhibit CAs.[6] More recently, our team developed nanomolar-potent oligoEG- and PEG-based CA IX inhibitors, which could efficiently bind and kill hypoxic carcinomas over-expressing CA IX.[25] Consequently, we translated these EG-based carbonic anhydrase inhibitors onto AuNPs.

Thus, two carbonic anhydrase inhibitors (CAIs) targeting ligands, compounds **5** and **6**, were designed and synthesized for this study as shown in Scheme 1. We have selected the lipoic acid (LA) anchor, which can readily attach to gold surface through its disulfide moiety and that was used extensively in anchoring various materials on Au surface, including CA inhibitors and activators by one of us.[6–7, 34] A convergent strategy was chosen for the synthesis of both CAI conjugates. Thus, the synthesis of both compounds started from succinyl derivative **2**, readily available through the reaction of 2-amino-1,3,4-thiadiazole-5-sulfonamide **1** and succinic anhydride.[25] The succinyl derivative **2** contains the 2-amino-1,3,4-thiadiazol-5-sulfonamide scaffold that proved to be an efficient CAI pharmacophore in many CA inhibition studies,[17–19, 25] binding with high affinity to the catalytically active Zn ion in the active site of CA.

The linkers of compounds **5** and **6** were designed to contain different numbers of ethylene glycol (EG) units, either 3 EGs (short linker) or about 45 EGs (long linker, MW ~ 2000). It was expected that the linkers would contribute differently to the stabilization of the Au nanoparticles post-decoration with ligands **5** and **6** and to interaction with CA IX target.[35–38] Our PEGylated ligands with MW 2000 combine a good steric stabilization with a relative

small footprint, thus keeping the resulting Au nanoplatforms relatively small, to facilitate both efficient interaction with the CA IX epitope and tumor penetration.

Therefore, carboxylic acid moiety of succinyl aminosulfonamide **2** was activated with 2-chloro-4,6-dimethoxy-1,3,5-triazine (CDMT)/N-methylmorpholine (NMM) and reacted with 1,8-diamino-3,6-dioxahexane or with H2NPEG2kNH2, in DMF, at low temperature (Scheme 1).

The mono-substituted products **3** and **4** were purified from disubstituted side-products via flash chromatography and were reacted with CDMT/NMM activated lipoic acid in DMF to generate the final CAI ligands **5** and **6** in pure form, which were characterized by standard techniques. A lipoic acid-PEG2000 conjugate (LA-PEG2000) **8**, devoid of the CAI warhead, was also synthesized as an inert conjugate to be used in control formulations via a similar synthetic strategy involving the activation of lipoic acid with CDMT/NMM and subsequent reaction with H2N-PEG2000OCH3 in DMF (Scheme 1).

Au NPs synthesis and characterization.

Within our nucleic acid delivery research program,[39] we reliably synthesized monodispersed Au NPs ~ 20 nm in diameter via the Turkevich method [31] and we performed ligand exchange with pyridinium thiols or disulfides to yield narrowly dispersed Py-Au NPs (D ~ 25 nm).[11] This AuNP size ensures much longer circulation times in vivo than the very small (3–5 nm), which are quickly removed from vasculature via glomerular filtration.[40] We used the same optimized Turkevich method, involving the reduction of HAuCl4 with citrate at high temperature,[31] to generate the Au NPs for this study. Immediately after preparation, the Au NPs were filtered through 0.22 μm membrane filter to remove large aggregates and the excess citrate was removed by pelleting the Au NPs and washing them with DI water containing small amount of NaOH. The size of the generated Au NPs was around 25 nm, with a negative zeta potential of around −20 mV due to surface citrate ligands. After removing the loosely bound citrate from Au NPs surface, the UV max for the generated Au NPs was found to be 520 nm, which correlates perfectly with the size of the gold nanoparticles.[41] The images acquired by the TEM confirmed the gold nanoparticles size and quasi-spherical morphology (Figure S1).

Targeting ligand exchange on Au NPs.

Subsequently, we employed our optimized targeting ligand exchange protocols to exchange citrate with a thiol or disulfide group on the surface of the Au NPs.[11] Four different ligands were used to decorate the gold surface: the two lipoic acid-CAI ligands having different ethylene glycol chain lengths LA-CAI **5** and LA-PEG2000-CAI **6**, the lipoic acid-polyethylene glycol 2000 conjugate LA-PEG2000 **8** and the simple lipoic acid (LA). We were able to generate colloidal stable functionalized Au NPs with physicochemical properties perfectly correlated with the type and nature of the targeting ligands that decorated the surface (Figure 1). The size of the functionalized AuNPs was slightly bigger than the citrate capped gold nanoparticles (32 nm) (Figure 1a). The surface ligands dictated the zeta potential of the corresponding Au NPs (Figure 1b). Thus, the LA decorated Au NPs showed a highly negative zeta potential due to the ionization of the lipoic acid carboxylic

groups, which provide electrostatic stabilization of the Au colloid. The LA-PEG2000 decorated Au NPs had a zeta potential of around 0 mV since PEG provides steric stabilization. For the CAI ligands decorated Au NPs, the zeta potential was also negative due to partial ionization of the sulfonamide group of the CAI moiety. The surface plasmon for the functionalized Au NPs (Figure 1c) showed a slight bathochromic shift as compared to the citrate capped Au NPs. This bathochromic shift correlates with the slight increase in size for the functionalized Au NPs observed by DLS. The shift was 2 nm for the nanoparticles decorated with short ligands and 4 nm for the particles decorated with long PEGylated ligands. TEM revealed that all functionalized Au NPs maintained the quasi spherical morphology similar to parent citrate Au NPs, which proves that ligand decoration did not affect the shape of the nanoparticles (Figure 1d).

The presence of targeting CAI ligands on the surface of Au NPs was also confirmed via a well-established inhibition assay of CA using the 4-nitrophenylacetate as substrate[17, 42] (Figure S2). This assay allows the quantitation of CA inhibition in a similar manner to the CO2 hydration assay but avoids absorbance interference of Au NPs (red) with the indicator (phenol red) used in the later assay. Acetazolamide, a potent CA inhibitor, was used as a positive control.[17, 42] Data from Figure S2 confirmed the efficient inhibition of CA with the CAI-decorated Au NPs. The inhibition potency was not significantly influenced by the linker length. Thus, AuNPs decorated with targeting CAI via short linkers displayed about the same inhibition potency as the similar AuNPs having long PEG linkers between LA gold anchor and targeting CAI ligands, equivalent to the 2.5 μM acetazolamide stock solution. Au NPs that did not have the CAI ligands on their surface did not inhibit the CA, as expected.

Interaction of CAI-decorated Au NPs with CA IX-expressing tumor cells.

For cell culture studies, we used the colorectal cancer cell line HT-29 as a model of tumor hypoxia.[25,43] The overexpression of CA IX under hypoxic conditions was validated by western blotting, where CA IX is known to have a characteristic twin band at 54 and 58 KDa.[44] As one can notice, the level of CA IX expression was significantly higher under hypoxic conditions as compared to normoxic conditions as shown in Figure 2a.

The uptake of the CAI-decorated Au NPs by HT-29 cancer cell lines was studied both quantitatively by ICP-OES technique (Figure 2b) as well as qualitatively through silver staining of Au NPs internalized by tumor cells (Figure 2c). Upon examination of Figure 2, one may notice that LA-decorated Au NPs (Au NPs-LA) were taken in large amounts by HT-29 cells under normoxic conditions. This high non-specific uptake is probably correlated with their size, which is right in the range of clathrin-mediated endocytosis,[45–46] known to be enhanced in cancer cells. The uptake was dramatically diminished under hypoxic conditions, probably due to a reduced metabolism.[47] Interestingly, the Au NPs decorated with short CAI ligands (Au NPs-LA-CAI) had a similar uptake to Au NPs-LA, as expected, since the size and zeta potential of the two Au NPs formulations are quite similar to Au NPs-LA and CA IX expression level is low under normoxic conditions. However, under hypoxic conditions the uptake was increased as compared to normoxia. Although non-statistically significant versus normoxia, the uptake of Au NPs-LA-CAI was much larger, in a statistically significant manner ($P < 0.01$), versus Au NPs-LA uptake under hypoxic

conditions. In contrast, PEGylated Au NPs (Au NPs-LA-PEG2000) displayed a very low uptake in both normoxic and hypoxic conditions. This is most probably due to the steric stabilization of PEG2000, which eliminates non-specific uptake and interactions with any proteins and receptors, and to the zeta potential of this nanoplatform, which is close to zero (Figure 1b).[48] When CAI ligands were introduced on the surface of PEGylated Au NPs (Au NPs-LA-PEG2000-CAI), one would observe a small uptake by HT-29 cells under normoxic conditions. Since PEGylation drastically reduces the non-specific uptake, the observed internalization is most probably due to the CA IX-mediated endocytosis,[38, 49] mediated by the small amounts of this protein present on the surface of HT-29 cells even under normoxic conditions (Figure 2a). Importantly, AuNPs-LA-PEG2000-CAI showed significantly higher cell uptake under hypoxic conditions versus normoxia, a fact that we correlate to the high expression of CA IX under hypoxic conditions by the HT-29 cancer cells and CA-IX mediated endocytosis of the Au NPs. The AuNPs-LA-PEG2000-CAI are clearly more selective for CA IX-expressing, hypoxic HT-29 cells than the particles decorated with short chain ethylene glycol ligands AuNPs-LA-CAI. This difference proves the importance of the PEG spacer for eliminating non-specific uptake and optimum interaction with CA IX target. Consequently, the relatively high non-specific uptake of AuNPs-LA-CAI under normoxia and the modest increased uptake under hypoxia of these targeted nanocarriers put them at disadvantage versus the PEGylated ones (AuNPs-LA-PEG2000-CAI) that have very low non-specific absorption and are selectively uptaken only when the CAI ligands are present and CA IX target is overexpressed by the hypoxic HT-29 cancer cells. The quantitative results (Figure 2b) are clearly mirrored by the qualitative ones generated by silver staining of Au NPs internalized by the tumor cells via silver benzoate (Figure 2c).

Once the uptake of Au NPs was confirmed, we proceeded in testing the cytotoxicity of these Au NPs on the same HT-29 colon cancer cell line following a 24 h exposure under normoxic or hypoxic conditions (Figure 3). Data from Figure 3 reveals that exposing the cells to the Au NPs did not generate any significant toxicity under normoxic conditions, irrespective of the type of Au NPs or their concentration. Under hypoxic conditions, only Au NPs decorated with PEG2000-CAI targeting ligand (Au NPs-LA-PEG2000-CAI) proved to be able to kill HT-29 cells in a statistically significant manner and this tumor cell killing occurred only at the highest concentration of 100 μM. We postulate that this is due to the efficient inhibition of the overexpressed CA IX by the CAI targeting moiety of these Au NPs, similarly to our CA polymeric inhibitors from which our targeting ligands derived. The cell killing shown by Au NPs-LA-PEG2000-CAI was due to the presence of the long PEG2000 spacer between the CAI warhead and the surface of the Au NPs. We postulate that the long (and coiled) PEG spacer places the CAI warheads at a lateral distance which is better suited to engage the CA IX, which is a dimeric protein. This finding is in agreement with our previous work, in which we also observed that the presence of PEG2000 between two CAI warheads enhances the binding and cell killing of CAI moieties as compared to short linkers.[25]

Summarizing the data from Figures 2 and 3, one can observe that Au NPs-LA and Au NPs-LA-CAI did not produce any statistically-significant cytotoxic effect, despite the relatively high (non-selective) uptake of these NPs by HT-29 cells, under both normoxic and hypoxic conditions. This prompted us to abandon these nanoplatforms and focus our delivery efforts

to the PEGylated ones, which have very low non-specific absorption, are endocytosed only when decorated with CAI, and are able to also contribute to tumor cell killing via efficient CA IX inhibition. We decided to use these CA IX targeted Au NPs as a nanoplatform for the delivery of doxorubicin, by combining the excellent CA IX targeting capabilities of Au NPs-LA-PEG2000-CAI with the high toxicity of doxorubicin.

At this point, mention must be made that CA IX was used successfully for targeted delivery of drug cargos[50] to tumors and for tumor imaging.[51–54] Importantly, it was recently shown that although hypoxia downregulates constitutive endocytosis in tumor cells, conjugates targeting CA IX can still be efficiently and specifically internalized under hypoxic conditions, resulting in selective delivery of conjugates to hypoxic tumor cells.[55]

Focusing on the drug cargo, it must be emphasized that doxorubicin (Dox) is considered to be one of the most effective chemotherapeutic drugs, making it a first line treatment to cure many types of cancer such as lung, breast, ovaries and multiple myeloma.[56–57] It acts through intercalating into DNA and also inhibits topoisomerase II, responsible for relaxing of supercoiled DNA, thus preventing DNA transcription and translation. Doxorubicin was also proved to promote the formation of free radicals, causing oxidative damage to DNA, proteins and cell membrane lipids.[58] Due to this complex mechanism of action, the drug is very toxic for normal cells. Severe side effects have been associated with the IV administration of free doxorubicin, especially dose-dependent cardiotoxicity, myelosuppression, mucocutaneous reactions, nausea, vomiting and hyperpigmentation of the skin.[59] These premises raise the demand to deliver the drug to the tumor cells in a selective manner, which we believed it could be ensured by our proposed Dox-loaded Au NPs targeted against CA IX epitope over-expressed in hypoxic tumors.

Therefore, we initiated a synthetic program to identify the most efficient ways to load doxorubicin on the Au NPs-LA-PEG2000-CAI nanoplatform.

Design and loading of doxorubicin conjugates on Au NPs.

We assessed several different strategies to maximize the loading of doxorubicin (Dox) on Au NPs, while preserving their physicochemical properties (Chart 1). These strategies were based on doxorubicin conjugates having different Au anchoring ligands such as lipoic acid (LA) or 3,3’-dithiodipropionic acid (DTDP). We started our investigations by exploring conjugates in which the drug was attached through a stable amide (AM) linker to the Au ligand (see experimental section). The first conjugate, LA-AM-Dox, proved to have a poor water solubility and failed to generate stable gold nanoparticles. On the other hand, the solubility of DTDP-doxorubicin amide conjugate (DTDP-AM-Dox) was quite good in water/ethanol mixtures and we were able to generate gold nanoparticles Dox-AM-DTDP @ Au NPs-LA-PEG2000 (Scheme S5, Figure S3). Moreover, DTDP is a more efficient conjugation ligand than LA since it allows the loading of two Dox molecules per one ligand unit. Thus, two strategies were used to load DTDP-AM-Dox conjugate onto Au NPs: a simultaneous strategy in which the Dox conjugate was pre-mixed with LA-PEG2000 (CAI) ligand, then co-incubated with citrate Au NPs, and a sequential strategy in which first the LA-PEG2000 (CAI) conjugate was installed on the gold surface followed by incubation of

Au NPs-LA-PEG2000 (CAI) with excess Dox-AM-DTDP. We started with the cheaper, non-targeted PEGylated ligand **8** in the optimization of the Dox-loading process (Scheme S5).

Using the above pre-optimized simultaneous strategy and parameters, we were also able to generate the corresponding CAI targeted nanosystems Dox-AM-DTDP @ Au NPs-LA-PEG2000-CAI (see Methods section and Supporting Information).

In an alternative conjugation strategy, we attempted to attach the doxorubicin on the same dithiodipropionic acid and on related thioglycolic acid anchoring ligands using a hydrolysable hydrazone linker, which was used successfully by other groups for the same purposes.[14,16–61] The hydrazone linker was generated either in situ, by reacting Au NPs pre-decorated with hydrazide containing ligands with excess Dox in solution, or was generated synthetically (before decoration) and subsequently added onto Au NPs (Scheme S6).

Thus, in the initial in situ loading strategy, the Au NP were decorated with methylthioglycolate (MeTG) followed by addition of hydrazine to transform the ester in the hydrazide and subsequently with doxorubicin to react with the hydrazide yielding the loaded Au NPs.[62] Again, a sequential or simultaneous addition formulation attempts were done (Figure S4).

The sequential strategy yielded large aggregates and was abandoned. On the other hand, the simultaneous strategy generated a more stable and homogenous formulation (Scheme S6). This formulation was treated with excess hydrazine hydrate to generate the HZD-TG @ Au NPs-LA-PEG2000 bearing hydrazide ligands on the Au NPs, which was characterized by standard methods (Figure S4). Subsequent treatment of these Au NPs with excess doxorubicin generated the desired Dox-HZN-TG @ Au NPs-LA-PEG2000. Unfortunately, this formulation proved unstable and flocculated during the cleaning procedure, in the centrifugation step (see Methods section). We believed that the colloidal instability of these Dox loaded Au NPs was due to insufficient steric stabilization of Au NPs by the PEG corona. We hypothesized that the TG anchor partially removes the LA-anchored PEG, especially when the TG conjugate is used in excess. This explanation could account also for the failures observed in preparation of Au NPs via the sequential strategy.

Consequently, we have decided to switch towards a dithiodipropionic acid (DTDP) Au anchoring ligand, as this ligand is also of disulfide type similar to LA and LA-terminated ligands. Two DTDP ligands were made for this purpose, DTDP-hydrazide (DTDP-HZD) and the preformed Dox hydrazone conjugate with DTDP (DTDP-HZN-Dox, see experimental section). Both ligands were installed on Au NPs together with the PEGylated ones using the simultaneous strategy proved efficient for generation of Au NP conjugates described above (Scheme S7).

The DTDP-HZD conjugate was placed on Au NPs simultaneously with LA-PEG2000, pre-mixed with it at two different ratios (1:1 and 3:1 DTDP:LA conjugates). Following the cleaning procedure, the stable Au NPs were treated with excess doxorubicin for 24 h at room temperature. After cleaning and removing the unbound free drug, the doxorubicin loaded Au NPs were characterized in terms of size, zeta potential and plasmon spectrum (Figure S5)

Data from Figure S5 showed that loading of doxorubicin did not affect significantly the size of Au NPs but it clearly influenced their zeta potential, which became positive (around +15 mV) in both cases since the amino group of doxorubicin is positively charged. The zeta potential shift from negative to positive values was possible because of the LA-PEG2000 ligand which sterically stabilized the Au NPs when zeta potential passed through a zero value. The UV-Vis spectrum of the Au NPs revealed a shift in the main peak from 520 nm to 526 nm in both cases giving another indication for Dox loading. It is known that Dox self-quenches when loaded on Au NPs since the emission band of Dox overlaps with the absorbance band of the Au NPs and the resulting spectrum is the contribution of the two (vide infra).[9, 60] In order to validate Dox loading and to quantitate the loading amount of Dox on the Au NPs, the two Dox loaded Au NPs were treated with 0.1 N HCl in order to liberate the free drug, which was quantified via fluorescence spectroscopy. The results (Figure 4) confirmed the Dox loading and the success of this on-bead drug conjugation strategy. One may observe that tripling the amount of DTDP-HZD in the initial mixture from (1:1 molar ratio to LA-PEG2000 to 3:1 molar ratio) did not translate into an increase in Dox loading. Another observation was the Dox loading of these Au NPs was relatively low. We believe that the low Dox loading was due to suboptimal loading kinetics: once some Dox was loaded to the Au NPs, the positively charged Dox ligand layer could electrostatically repel other incoming positively charged Dox molecules, preventing further Dox loading onto the Au NPs.

Consequently, in an attempt to maximize the loading of Dox, we synthesized an original DTDP-hydrazone-doxorubicin conjugate (Dox-HZN-DTDP, see Supporting Information). This conjugate was premixed with LA-PEG2000 at four different ratios and the mixtures were added to the Au NPs to successfully generate stable Dox-HZN-DTDP @ Au NPs-LA-PEG2000. The physiochemical parameters of Dox-HZN-DTDP @ Au NPs- LA-PEG2000 are shown in Figure S6. One can observe from Figure S6 that increasing the ratio (and amount) of Dox conjugate in the ligand mixture did not affect the size or the zeta potential of the Dox loaded Au NPs. Zeta potential shifted from negative to positive values, as in the previous on-bead drug loading strategy.

Mention must be made that the zeta potential of all four Au NPs formulations was significantly higher than in the previous strategy, hinting towards more drug loaded onto Au NPs. Hydrolysis of hydrazone and quantification of liberated Dox as previously described revealed that this strategy yielded indeed the highest Dox loading, with a threefold increase in drug loading as compared to previous on-bead loading strategy (Figure 4). A higher initial molar ratio of LA-PEG2000/Dox-HZN-DTDP did not translate into higher Dox loading (Figure 4). Therefore, for loading of Au NP bearing CAI ligands only the most economical 1:1 ligand ratio was used, yielding Dox-HZN-DTDP @ Au NPs-LA-PEG2000-CAI formulation. A Dox loading of approximately 22.7 μg/ml was revealed after acid mediated hydrolysis of hydrazone linker, showing that the CAI ligand does not affect the loading of the Dox via its conjugate.

As mentioned above, it is known that loading of Dox onto Au NPs results in quenching of Dox fluorescence signal (see also Figure S7).[9, 60] On the other hand, when the hydrazone linker is cleaved and Dox is released, the fluorescence signal is retrieved and intensifies with

more drug being released. Therefore, to validate that the cleavage of the hydrazone linker and the subsequent release of Dox is pH dependent, we incubated both Dox-HZN-DTDP @ Au NPs-LA-PEG2000-CAI **(THZN)** and Dox-HZN-DTDP @ Au NPs-LA-PEG2000 **(NTHZN)** in phosphate buffer saline at either pH 5.5 or pH 7.4, over a period of 24 h, and recorded the emission spectra at different time intervals (Figure S8). One may observe in Figure S8 that at pH 5.5, there is a rapid increase in the fluorescence intensity of Dox with time for both NTHZN and THZN. However, at pH 7.4, there was no significant increase in fluorescence intensity over the entire period of 24 h.

We also quantitated the percentage of Dox released from both NTHZN and THZN after incubation in PBS at pH 5.5 or pH 7.4, over a period of 24 h (Figure S9). Data from Figure S9 revealed that at pH 5.5 there was a burst release of Dox from both NTHZN and THZN with almost 80% of the loaded drug released after 4h and 98% of the loaded drug released after 24 h. On the other hand, at pH 7.4, both NTHZN and THZN demonstrated a very slow release rate of Dox with < 20 % of the loaded drug released after 4h and only 23 % of the loaded drug released after 24 h. These results confirm that the release of Dox from the Au NPs is pH dependent and validate our control release model.

Tumor cell killing of the Dox-loaded Au nanoplatforms

We re-analyzed for cytotoxic effects of the new doxorubicin loaded Au NPs, having the Dox attached to the Au anchoring moiety either via an amide group (Dox-AM-DTDP) or via a hydrazone group (Dox-HZN-DTDP). The amide group is stable over a wide range of pH, while the hydrazone group is cleaved at pH of late endosome (pH = 5.5, validated in Figure S8). Formulations included the targeting moiety **(T)** LA-PEG2000-CAI and just the LA-PEG2000 non targeted **(NT)** ones; Dox-AM-DTDP @ Au NPs-LA-PEG2000 **(NTAM),** Dox-HZN-DTDP

Au NPs-LA-PEG2000 **(NTHZN),** Dox-AM-DTDP @ Au NPs-LA-PEG2000-CAI **(TAM)**, Dox-HZN-DTDP @ Au NPs-LA-PEG2000-CAI **(THZN)**.

We tested these Dox loaded Au NPs on the same HT-29 cell model expressing CA IX under normoxic and hypoxic conditions in similar conditions to the non-loaded Au NPs presented before. As controls we added the non-loaded Au NPs-LA-PEG2000 and Au NPs-LA-PEG2000-CAI formulations prepared in the same conditions. Prior to incubation with cells, all the formulations were also assessed for the Au content via ICP-OES and their concentration was adjusted with media to yield a final Au concentration in media of 100 μM. Under these conditions, the amount of Dox in the **NTHZN** and **THZN** formulations were assessed and found to be approximately 2.2 μg/ml. Consequently, a free Dox control was made at the same concentration.

The viability results of HT-29 cells treated with above mentioned formulations are presented in Figure 5. Data from Figure 5 shows that there is a statistically-significant reduction in the cytotoxicity of free Dox, under hypoxic conditions (50% cell viability) as compared to normoxic ones (41% cell viability), as previously reported,[63–64] due to the suppression of ROS-mediated toxicity mechanism of Dox under hypoxic conditions.[65] The control formulations Au NPs-LA-PEG2000 and Au NPs-LA-PEG2000CAI duplicated the same

toxicity profile showed in Figure 3 with the Au NPS-LA-PEG2000CAI having a significant toxicity under hypoxic conditions due to its inhibitory effect on CA IX that is overexpressed under hypoxic conditions. The Au NPs-LA-PEG2000 did not show any cytotoxic effect under both normoxic and hypoxic conditions, confirming the results of Figure 3 and supporting the use of PEGylated Au NPs as an ideal nanoplatform for delivery of drugs.[35] The Dox loaded formulations bearing the drug linked via an amide group did not show any additional cytotoxic effects to their non-targeted or CA IX targeted nanoplatforms. This is possibly due to the stability of the amide group that does not release the drug fast enough to induce any significant cytotoxic effects. On the other hand, the Dox formulations bearing the pH-labile hydrazone group showed an improved cytotoxicity compared with their unloaded delivery platforms under both normoxic and hypoxic conditions. This was due to the fast cleavage of acid sensitive hydrazone linker in the late endosome following the uptake of the nanoparticles, thus liberating free Dox in large amounts, which killed the cells in a significant manner. Interestingly, the toxicity of the **(NTHZN)** was reduced under hypoxic conditions versus normoxic ones, similarly to the free Dox ($P < 0.05$). Most importantly, the CA IX targeted **(THZN)** formulations showed superior cytotoxic effects as compared to **NTHZN** formulations. We postulate that this is due to the contribution of CA IX in facilitating the uptake and the internalization of the nanoparticles. In case of normoxic conditions, the cell viability dropped significantly from 70% for the **NTHZN** to 59% for the **THZN** while under hypoxic conditions the cell viability dropped from 76% for the **NTHZN** to 57% for the **THZN**. Moreover, one can observe that the toxicity of **THZN** NPs was slightly higher in hypoxia than in normoxia, reversing the hypoxia-induced chemoresistance observed for non-targeted NPs and for free Dox. It is also clear that the cytotoxicity of **THZN** under hypoxic conditions was comparable with free Dox under hypoxic conditions. This significant drop in tumor cell viability reveals the potentiating role of CA IX, overexpressed in hypoxia, to enhance the uptake of the targeted formulations, which translates in the liberation of a higher amount of free drug in a controlled fashion inside the tumor cells, thus supporting our working hypothesis.

Uptake and intracellular trafficking of the Dox-loaded Au nanoplatforms

We confirmed this mechanism via confocal microscopy, incubating HT-29 cancer cells transfected with Rab7-GFP with the **NTHZN** or **THZN** Au nanoplatforms, under hypoxic conditions, for either 4h or 24h. (Figure 6). The Rab-7 GTPase is a protein specific for endolysosomes that is absent in caveolae and in vesicles internalized from plasmalemma.[66–67] Its fusion with GFP allows the identification of endolysosomes inside the target cells. An analysis of images from Figure 6 confirmed that **THZN** nanoplatforms were significantly endocytosed and accumulated within the lysosomes of HT-29 cells after 4 h as compared to **NTHZN**. We postulate this effect is due to the overexpression of CA IX under hypoxic conditions, which enhances the cell uptake of THZN, while the NTHZN nanoplatform exhibited limited endocytosis, probably driven by their positively-charged zeta potential (Figure S6). Moreover, at this time, the Dox started to be released from the Au NPs and it was mainly localized within the lysosomes. It could be observed that the intensity of Dox signal from **THZN** was greater than from **NTHZN**, which reflects the higher uptake of the targeted formulation **THZN** as compared with the non-targeted **NTHZN** one bearing the same pH-sensitive linker. After 24 h, in addition to Dox localization in the lysosomes, one

could also observe a diffuse Dox signal in the cytoplasm of (still viable) HT-29 cells. The intensity of the Dox signal was again much higher in the case of **THZN** nanoplatform versus **NTHZN** one, reflecting the essential contribution of CA IX-mediated internalization under hypoxic conditions. Importantly, a significant decrease in the number of cell colonies for HT-29 cell lines was noticed, as a result of Dox-mediated tumor cell killing (Figure 6).

Delivery of doxorubicin into HT-29 tumor spheroids via gold nanoplatforms and comparison with free drug administration

In order to test the behaviour of our doxorubicin-loaded Au nanoplatforms into a model closer to the real hypoxic tumors, we generated HT-29 tumor spheroids as previously described.[25, 33] These spheroids are becoming hypoxic due to their uncontrolled 3D growth which prevents penetration of oxygen into the core of the spheroid. As a consequence CA IX is strongly induced, as proved by us previously using this 3D hypoxic tumor model by western blotting using the CA IX selective antibody M75.[25] Spheroids were treated with either free doxorubicin (5 μg/mL), with **NTHZN** and **THZN** gold nanoplatforms, containing the same doxorubicin concentration, for 1 h treatment period. Following extensive washing with PBS, the amount of doxorubicin delivered into the tumor spheroids was quantified by confocal fluorescence microscopy and by fluorescence spectroscopy (see experimental section).

Confocal fluorescence microscopy revealed a strikingly different distribution of doxorubicin into the hypoxic tumor spheroids (Figure 7a). Thus, data from Figure 7a reveals that in the case of free Dox the drug is confined to the periphery of the spheroid, in agreement with previous reports.[68–69] This is probably due to the combined effect of lipophilicity of Dox and the mild acidic environment (pH ~ 6.5–6.9) generated by hypoxia inside the solid tumors,[24, 70] which partially protonates the basic drugs, making them positively charged. The tumor penetrability of the (partial) positively charged lipophilic drug remains very low, as observed in Figure 7a and in other literature studies.[68−69]

On the other hand, the Au nanoplatforms protect the drug from the (weakly) acidic environment and, due to their relatively small size, are able to penetrate better through the tumor. In this context we observed that the **NTHZN** nanoplatform exhibited a better tumor penetration profile as compared to free Dox. Our quantitative assay revealed that the total amount of drug delivered to the tumor spheroid, normalized by protein content, was about about the same as in the case of free Dox (Figure 7b), due to limited internalization of the **NTHZN** nanoplatform, despite the better tumor penetration than free Dox. In contrast, the **THZN** nanoplatform showed better tumor penetration and doxorubicin delivery as compared to both **NTHZN** and free Dox. Our THZN nanoplatform combines transport of Dox inside the microtumor with efficient internalization and controlled delivery into cytoplasm, and was able to deliver more Dox as compared to NTHZN due to the essential contribution of CA IX-mediated uptake. Importantly, assessment of total drug delivered to the tumor spheroids by fluorescence spectroscopy revealed that **THZN** nanoplatform delivered almost 2.5 times more doxorubicin than both **NTHZN** nanoplatform or free Dox treatment (Figure 7b). We postulate that the **THZN** nanoplatform reduces Dox resistance as

it allows efficient intracellular delivery of more Dox, in a controlled fashion, to the tumor cells.

Conclusions

We optimized a CA IX targeted gold nanoplatform for efficient doxorubicin delivery to hypoxic tumors. We designed compatible CAI- and Dox- ligands, and optimized protocols for AuNPs efficient decoration to achieve both good targeting ligand density and optimum drug loading, while preserving colloidal stability of the nanoplatform.

The optimized Dox-HZN-DTDP @ Au NPs-LA-PEG2000-CAI (THZN) nanoplatform proved to be very efficient towards killing HT-29 tumor cells especially under hypoxic conditions, reducing the hypoxia-induced chemoresistance, and exhibiting a better tumor penetration profile and intratumoral doxorubicin delivery as compared to free Dox. These findings reveal the potentiating role of CA IX, overexpressed in hypoxia, to enhance the uptake of the targeted nanoformulations, and recommend our CA IX-targeted nanoplatform as a compelling nanotechnology to increase delivery of basic chemotheraputic drugs, reduce hypoxia-induced chemoresistance and maximize tumor killing, with the perspective to improve the therapy of solid tumors.

Supplementary Material

Refer to Web version on PubMed Central for supplementary material.

Acknowledgements

The financial support of Temple Drug Discovery Initiative, NIH (R03EB026189), NSF (CHE-0923077), TUSP Dean's Office, Temple Undergraduate Research Program is gratefully acknowledged, Authors wish to thank Drs. Daniel Strongin, Kayleigh Jones, Lauren Profit, Samantha Shumlas for their help and support towards the TEM and ICP-OES characterization of Au NPs presented here and to Drs. Salim Merali, George Mateo and Bogdan Draghici for their support towards MALDI-TOF analysis.

References

1. Sperling RA; Rivera Gil P.; Zhang F; Zanella M; Parak WJ, Biological Applications of Gold Nanoparticles. Chem. Soc. Rev 2008, 37 (9), 1896–1908. [PubMed: 18762838]
2. Dreaden EC; Alkilany AM; Huang X; Murphy CJ; El-Sayed MA, The Golden Age: Gold Nanoparticles for Biomedicine. Chem. Soc. Rev 2012, 41 (7), 2740–2779. [PubMed: 22109657]
3. Saha K; Agasti SS; Kim C; Li X; Rotello VM, Gold Nanoparticles in Chemical and Biological Sensing. Chem. Rev 2012, 112 (5), 2739–2779. [PubMed: 22295941]
4. Giljohann DA; Seferos DS; Daniel WL; Massich MD; Patel PC; Mirkin CA, Gold Nanoparticles for Biology and Medicine. Angew. Chem., Int. Ed. Engl 2010, 49 (19), 3280–3294. [PubMed: 20401880]
5. Huang X; El-Sayed MA, Gold Nanoparticles: Optical Properties and Implementations in Cancer Diagnosis and Photothermal Therapy. J. Adv. Res 2010, 1 (1), 13–28.
6. Stiti M; Cecchi A; Rami M; Abdaoui M; Barragan-Montero V; Scozzafava A; Guari Y; Winum JY; Supuran CT, Carbonic Anhydrase Inhibitor Coated Gold Nanoparticles Selectively Inhibit the Tumor-Associated Isoform IX Over the Cytosolic Isozymes I and II. J. Am. Chem. Soc 2008, 130 (48), 16130–16131. [PubMed: 18989963]
7. Saada MC; Montero JL; Vullo D; Scozzafava A; Winum JY; Supuran CT, Carbonic Anhydrase Activators: Gold Nanoparticles Coated with Derivatized Histamine, Histidine, and Carnosine Show

Enhanced Activatory Effects on Several Mammalian Isoforms. J. Med. Chem 2011, 54 (5), 1170–1177. [PubMed: 21291238]

8. Ghosh P; Han G; De M; Kim CK; Rotello VM, Gold Nanoparticles in Delivery Applications. Adv. Drug Delivery Rev 2008, 60 (11), 1307–1315.
9. Kang B; Afifi MM; Austin LA; El-Sayed MA, Exploiting the Nanoparticle Plasmon Effect: Observing Drug Delivery Dynamics in Single Cells via Raman/Fluorescence Imaging Spectroscopy. Acs Nano 2013, 7 (8), 7420–7427. [PubMed: 23909658]
10. Rosi NL; Giljohann DA; Thaxton CS; Lytton-Jean AK; Han MS; Mirkin CA, Oligonucleotide-Modified Gold Nanoparticles for Intracellular Gene Regulation. Science 2006, 312 (5776), 1027–1030. [PubMed: 16709779]
11. Kizewski A; Ilies MA, Efficient and Synergetic DNA Delivery with Pyridinium Amphiphiles-Gold Nanoparticle Composite Systems having Different Packing Parameters. Chem. Commun. (Cambridge, U. K.) 2016, 52 (1), 60–63.
12. Cygan MT; Dunbar TD; Arnold JJ; Bumm LA; Shedlock NF; Burgin TP; Jones L; Allara DL; Tour JM; Weiss PS, Insertion, Conductivity, and Structures of Conjugated Organic Oligomers in Self-Assembled Alkanethiol Monolayers on Au{111}. J.Am. Chem. Soc 1998, 120 (12), 2721–2732.
13. Popovtzer R; Agrawal A; Kotov NA; Popovtzer A; Balter J; Carey TE; Kopelman R, Targeted Gold Nanoparticles Enable Molecular CT Imaging of Cancer. Nano Lett 2008, 8 (12), 4593–4596. [PubMed: 19367807]
14. Morshed RA; Muroski ME; Dai Q; Wegscheid ML; Auffinger B; Yu D; Han Y; Zhang L; Wu M; Cheng Y; Lesniak MS, Cell-Penetrating Peptide-Modified Gold Nanoparticles for the Delivery of Doxorubicin to Brain Metastatic Breast Cancer. Mol. Pharmaceutics 2016, 13 (6), 1843–1854.
15. Hanahan D; Weinberg RA, Hallmarks of Cancer: The Next Generation. Cell 2011, (5), 646–674. [PubMed: 21376230]
16. Gillies RJ; Gatenby RA, Metabolism and Its Sequelae in Cancer Evolution and Therapy. Cancer J 2015, 21 (2), 88–96. [PubMed: 25815848]
17. Supuran CT, Carbonic Anhydrases: Novel Therapeutic Applications for Inhibitors and Activators. Nat. Rev. Drug Discovery 2008, 7, 168–181. [PubMed: 18167490]
18. Akocak S; Ilies MA, Next-Generation Primary Sulfonamide Carbonic Anhydrase Inhibitors. In Targeting Carbonic Anhydrases, Supuran CT; Capasso C, Eds. Future Science: London, 2014, pp 35–51.
19. Neri D; Supuran CT, Interfering with pH Regulation in Tumours as a Therapeutic Strategy. Nat. Rev. Drug Discovery 2011, 10 (10), 767–777. [PubMed: 21921921]
20. Muz B; de la Puente P; Azab F; Azab AK, The Role of Hypoxia in Cancer Progression, Angiogenesis, Metastasis, and Resistance to Therapy. Hypoxia (Auckl) 2015, 3, 83–92. [PubMed: 27774485]
21. Svastova E; Hulikova A; Rafajova M; Zat'ovicova M; Gibadulinova A; Casini A; Cecchi A; Scozzafava A; Supuran CT; Pastorek J; Pastorekova S, Hypoxia Activates the Capacity of Tumor-Associated Carbonic Anhydrase IX to Acidify Extracellular pH. FEBS Lett 2004, 577 (3), 439–445. [PubMed: 15556624]
22. Alterio V; Hilvo M; Di Fiore A; Supuran CT; Pan P; Parkkila S; Scaloni A; Pastorek J; Pastorekova S; Pedone C; Scozzafava A; Monti SM; De Simone G, Crystal Structure of the Catalytic Domain of the Tumor-Associated Human Carbonic Anhydrase IX. Proc Natl Acad Sci U S A 2009, 106 (38), 16233–16238. [PubMed: 19805286]
23. Tafreshi NK; Lloyd MC; Bui MM; Gillies RJ; Morse DL, Carbonic Anhydrase IX as an Imaging and Therapeutic Target for Tumors and Metastases. Subcell. Biochem 2014, 75, 221–254. [PubMed: 24146382]
24. Wojtkowiak JW; Verduzco D; Schramm KJ; Gillies RJ, Drug Resistance and Cellular Adaptation to Tumor Acidic pH Microenvironment. Mol Pharmaceut 2011, 8 (6), 2032–2038.
25. Akocak S; Alam MR; Shabana AM; Sanku RK; Vullo D; Thompson H; Swenson ER; Supuran CT; Ilies MA, PEGylated Bis-Sulfonamide Carbonic Anhydrase Inhibitors Can Efficiently Control the Growth of Several Carbonic Anhydrase IX-Expressing Carcinomas. J. Med. Chem 2016, 59 (10), 5077–5088. [PubMed: 27144971]

26. Ilies MA; Vullo D; Pastorek J; Scozzafava A; Ilies M; Caproiu MT; Pastorekova S; Supuran CT, Carbonic Anhydrase Inhibitors. Inhibition of Tumor-Associated Isozyme IX by Halogenosulfanilamide and Halogenophenylaminobenzolamide Derivatives. J. Med. Chem 2003, 46 (11), 2187–2196. [PubMed: 12747790]
27. Rami M; Dubois L; Parvathaneni NK; Alterio V; van Kuijk SJ; Monti SM; Lambin P; De Simone G; Supuran CT; Winum JY, Hypoxia-Targeting Carbonic Anhydrase IX Inhibitors by a New Series of Nitroimidazole-Sulfonamides/Sulfamides/Sulfamates. J. Med. Chem 2013, 56 (21), 8512–8520. [PubMed: 24128000]
28. Mahon BP; Lomelino CL; Ladwig J; Rankin GM; Driscoll JM; Salguero AL; Pinard MA; Vullo D; Supuran CT; Poulsen SA; McKenna R, Mapping Selective Inhibition of the Cancer-Related Carbonic Anhydrase IX Using Structure-Activity Relationships of Glucosyl-Based Sulfamates. J. Med. Chem 2015, 58 (16), 6630–6638. [PubMed: 26203869]
29. Supuran CT; Scozzafava A; Ilies MA; Iorga B; Cristea T; Briganti F; Chiraleu F; Banciu MD, Carbonic Anhydrase Inhibitors - Part 53 - Synthesis of Substituted- Pyridinium Derivatives of Aromatic Sulfonamides: The First Non-Polymeric Membrane-Impermeable Inhibitors with Selectivity for Isozyme IV. Eur J Med Chem 1998, 33 (7–8), 577–594.
30. Scozzafava A; Briganti F; Ilies MA; Supuran CT, Carbonic Anhydrase Inhibitors: Synthesis of Membrane-Impermeant Low Molecular Weight Sulfonamides Possessing in Vivo Selectivity for the Membrane-Bound Versus Cytosolic Isozymes. J. Med. Chem 2000, (2), 292–300. [PubMed: 10649985]
31. Turkevich J; Stevenson PC; Hillier J, A Study of the Nucleation and Growth Processes in the Synthesis of Colloidal Gold. Discuss. Faraday Soc 1951, 11 (0), 55–75.
32. Zhang G; Tian M, A Rapid ICP-OES Strategy for Determination of Gold and Silver in Blister Copper by Nitric Acid Digestion. Opt. Spectrosc 2014, 116 (3), 365–367.
33. Sharma VD; Lees J; Hoffman NE; Brailoiu E; Madesh M; Wunder SL; Ilies MA, Modulation of Pyridinium Cationic Lipid-DNA Complex Properties by Pyridinium Gemini Surfactants and Its Impact on Lipoplex Transfection Properties. Mol Pharmaceut 2014, 11 (2), 545–559.
34. Nair LV; Nazeer SS; Jayasree RS; Ajayaghosh A, Fluorescence Imaging Assisted Photodynamic Therapy Using Photosensitizer-Linked Gold Quantum Clusters. Acs Nano 2015, 9 (6), 5825–5832. [PubMed: 25970038]
35. Pelaz B; del Pino P; Maffre P; Hartmann R; Gallego M; Rivera-Fernandez S; dela Fuente JM; Nienhaus GU; Parak WJ, Surface Functionalization of Nanoparticles with Polyethylene Glycol: Effects on Protein Adsorption and Cellular Uptake. Acs Nano 2015, 9(7), 6996–7008. [PubMed: 26079146]
36. Tirosh O; Barenholz Y; Katzhendler J; Priev A, Hydration of Polyethylene Glycol-Grafted Liposomes. Biophys. J 1998, 74 (3), 1371–1379. [PubMed: 9512033]
37. Shiraishi K; Sanada Y; Mochizuki S; Kawano K; Maitani Y; Sakurai K; Yokoyama M, Determination of Polymeric Micelles' Structural Characteristics, and Effect of the Characteristics on Pharmacokinetic Behaviors. J. Controlled Release 2015, 203, 77–84.
38. Ratto F; Witort E; Tatini F; Centi S; Lazzeri L; Carta F; Lulli M; Vullo D; Fusi F; Supuran CT; Scozzafava A; Capaccioli S; Pini R, Plasmonic Particles that Hit Hypoxic Cells. Adv. Funct. Mater 2015, 25 (2), 316–323.
39. Draghici B; Ilies MA, Synthetic Nucleic Acid Delivery Systems: Present and Perspectives. J. Med. Chem 2015, 58 (10), 4091–4130. [PubMed: 25658858]
40. Freese C; Anspach L; Deller RC; Richards SJ; Gibson MI; Kirkpatrick CJ; Unger RE, Gold Nanoparticle Interactions with Endothelial Cells Cultured Under Physiological Conditions. Biomater Sci-Uk 2017, 5 (4), 707–717.
41. Link S; El-Sayed MA, Size and Temperature Dependence of the Plasmon Absorption of Colloidal Gold Nanoparticles. J. Phys. Chem. B 1999, 103 (21), 4212–4217.
42. Alterio V; Di Fiore A; D'Ambrosio K; Supuran CT; De Simone G, Multiple Binding Modes of Inhibitors to Carbonic Anhydrases: How to Design Specific Drugs Targeting 15 Different Isoforms? Chem. Rev 2012, 112 (8), 4421–4468. [PubMed: 22607219]

43. Lv PC; Roy J; Putt KS; Low PS, Evaluation of a Carbonic Anhydrase IX-Targeted Near-Infrared Dye for Fluorescence-Guided Surgery of Hypoxic Tumors. Mol. Pharmaceutics 2016, 13 (5), 1618–1625.
44. Zavada J; Zavadova Z; Zat'ovicova M; Hyrsl L; Kawaciuk I, Soluble Form of Carbonic Anhydrase IX (CA IX) in the Serum and Urine of Renal Carcinoma Patients. Br. J. Cancer 2003, 89 (6), 1067–1071. [PubMed: 12966427]
45. Chithrani BD; Ghazani AA; Chan WC, Determining the Size and Shape Dependence of Gold Nanoparticle Uptake into Mammalian Cells. Nano Lett 2006, 6 (4), 662–668. [PubMed: 16608261]
46. Zhang S; Li J; Lykotrafitis G; Bao G; Suresh S, Size-Dependent Endocytosis of Nanoparticles. Adv. Mater 2009, 21, 419–424. [PubMed: 19606281]
47. Jain S; Coulter JA; Butterworth KT; Hounsell AR; McMahon SJ; Hyland WB; Muir MF; Dickson GR; Prise KM; Currell FJ; Hirst DG; O'Sullivan JM, Gold Nanoparticle Cellular Uptake, Toxicity and Radiosensitisation in Hypoxic Conditions. Radiother. Oncol 2014, 110 (2), 342–347. [PubMed: 24444528]
48. Soenen SJ; Manshian BB; Abdelmonem AM; Montenegro JM; Tan S; Balcaen L; Vanhaecke F; Brisson AR; Parak WJ; Smedt SCD; Braeckmans K, The Cellular Interactions of PEGylated Gold Nanoparticles: Effect of PEGylation on Cellular Uptake and Cytotoxicity. Part. Part. Syst. Charact 2014, 31 (7), 794–800.
49. Petrul HM; Schatz CA; Kopitz CC; Adnane L; McCabe TJ; Trail P; Ha S; Chang YS; Voznesensky A; Ranges G; Tamburini PP, Therapeutic Mechanism and Efficacy of the Antibody-Drug Conjugate BAY 79–4620 Targeting Human Carbonic Anhydrase 9. Mol. Cancer Ther 2012, 11 (2), 340–349. [PubMed: 22147747]
50. Krall N; Pretto F; Decurtins W; Bernardes GJ; Supuran CT; Neri D, A Small- Molecule Drug Conjugate for the Treatment of Carbonic Anhydrase IX Expressing Tumors. Angew. Chem., Int. Ed. Engl 2014, 53 (16), 4231–4235. [PubMed: 24623670]
51. Cecchi A; Hulikova A; Pastorek J; Pastorekova S; Scozzafava A; Winum JY; Montero JL; Supuran CT, Carbonic Anhydrase Inhibitors. Design of Fluorescent Sulfonamides as Probes of Tumor-Associated Carbonic Anhydrase IX that Inhibit Isozyme IX-Mediated Acidification of Hypoxic Tumors. J. Med. Chem 2005, 48 (15), 4834–4841. [PubMed: 16033263]
52. Ahlskog JK; Schliemann C; Marlind J; Qureshi U; Ammar A; Pedley RB; Neri D, Human Monoclonal Antibodies Targeting Carbonic Anhydrase IX for the Molecular Imaging of Hypoxic Regions in Solid Tumours. Br. J. Cancer 2009, 101 (4), 645–657. [PubMed: 19623173]
53. Pan J; Lau J; Mesak F; Hundal N; Pourghiasian M; Liu Z; Benard F; Dedhar S; Supuran CT; Lin KS, Synthesis and Evaluation of 18F-Labeled Carbonic Anhydrase IX Inhibitors for Imaging with Positron Emission Tomography. J. Enzyme Inhib. Med. Chem 2014, 29 (2), 249–255. [PubMed: 23463940]
54. Sneddon D; Niemans R; Bauwens M; Yaromina A; van Kuijk SJ; Lieuwes NG; Biemans R; Pooters I; Pellegrini PA; Lengkeek NA; Greguric I; Tonissen KF; Supuran CT; Lambin P; Dubois L; Poulsen SA, Synthesis and in Vivo Biological Evaluation of (68)Ga-Labeled Carbonic Anhydrase IX Targeting Small Molecules for Positron Emission Tomography. J. Med. Chem 2016, 59 (13), 6431–6443. [PubMed: 27322137]
55. Bourseau-Guilmain E; Menard JA; Lindqvist E; Indira Chandran V.; Christianson HC; Cerezo Magana M.; Lidfeldt J; Marko-Varga G; Welinder C; Belting M, Hypoxia Regulates Global Membrane Protein Endocytosis through Caveolin-1 in Cancer Cells. Nat. Commun 2016, 7, 11371. [PubMed: 27094744]
56. Minotti G; Menna P; Salvatorelli E; Cairo G; Gianni L, Anthracyclines: Molecular Advances and Pharmacologic Developments in Antitumor Activity and Cardiotoxicity. Pharmacological reviews 2004, 56 (2), 185–229. [PubMed: 15169927]
57. Duggan ST; Keating GM, Pegylated Liposomal Doxorubicin: A Review of its Use in Metastatic Breast Cancer, Ovarian Cancer, Multiple Myeloma and AIDS-Related Kaposi's Sarcoma. Drugs 2011, 71 (18), 2531–2558. [PubMed: 22141391]
58. Barenholz Y, Doxil(R)--The First FDA-Approved Nano-Drug: Lessons Learned. J. Controlled Release 2012, 160 (2), 117–134.

59. Tacar O; Sriamornsak P; Dass CR, Doxorubicin: An Update on Anticancer Molecular Action, Toxicity and Novel Drug Delivery Systems. The Journal of pharmacy and pharmacology 2013, 65 (2), 157–170. [PubMed: 23278683]
60. Wang F; Wang YC; Dou S; Xiong MH; Sun TM; Wang J, Doxorubicin-Tethered Responsive Gold Nanoparticles Facilitate Intracellular Drug Delivery for Overcoming Multidrug Resistance in Cancer Cells. Acs Nano 2011, 5 (5), 3679–3692. [PubMed: 21462992]
61. Xiao Y; Hong H; Matson VZ; Javadi A; Xu W; Yang Y; Zhang Y; Engle JW; Nickles RJ; Cai W; Steeber DA; Gong S, Gold Nanorods Conjugated with Doxorubicin and cRGD for Combined Anticancer Drug Delivery and PET Imaging. Theranostics 2012, 2 (8), 757–768. [PubMed: 22916075]
62. Aryal S; Grailer JJ; Pilla S; Steeber DA; Gong S, Doxorubicin Conjugated Gold Nanoparticles as Water-Soluble and pH-Responsive Anticancer Drug Nanocarriers. J. Mater. Chem 2009, 19 (42), 7879–7884.
63. Song X; Liu X; Chi W; Liu Y; Wei L; Wang X; Yu J, Hypoxia-Induced Resistance to Cisplatin and Doxorubicin in Non-Small Cell Lung Cancer is Inhibited by Silencing of HIF-1alpha gene. Cancer Chemother. Pharmacol 2006, 58 (6), 776–784. [PubMed: 16532342]
64. Sanna K; Rofstad EK, Hypoxia-Induced Resistance to Doxorubicin and Methotrexate in Human Melanoma Cell Lines in Vitro. Int. J. Cancer 1994, 58 (2), 258–262. [PubMed: 8026888]
65. Tredan O; Galmarini CM; Patel K; Tannock IF, Drug Resistance and the Solid Tumor Microenvironment. J. Natl. Cancer Inst 2007, 99 (19), 1441–1454. [PubMed: 17895480]
66. Wang TL; Ming Z; Wu XC; Hong WJ, Rab7: Role of its Protein Interaction Cascades in Endo-Lysosomal Traffic. Cell Signal 2011, 23 (3), 516–521. [PubMed: 20851765]
67. Yu J; Deliu E; Zhang XQ; Hoffman NE; Carter RL; Grisanti LA; Brailoiu GC; Madesh M; Cheung JY; Force T; Abood ME; Koch WJ; Tilley DG; Brailoiu E, Differential Activation of Cultured Neonatal Cardiomyocytes by Plasmalemmal Versus Intracellular G Protein-coupled Receptor 55. J Biol Chem 2013, 288 (31), 22481–22492. [PubMed: 23814062]
68. Kim TH; Mount CW; Gombotz WR; Pun SH, The Delivery of Doxorubicin to 3-D Multicellular Spheroids and Tumors in a Murine Xenograft Model Using Tumor-Penetrating Triblock Polymeric Micelles. Biomaterials 2010, 31 (28), 7386–7397. [PubMed: 20598741]
69. Perche F; Patel NR; Torchilin VP, Accumulation and Toxicity of Antibody-Targeted Doxorubicin-Loaded PEG-PE Micelles in Ovarian Cancer Cell Spheroid Model. J Control Release 2012, 164 (1), 95–102. [PubMed: 22974689]
70. Swietach P; Wigfield S; Cobden P; Supuran CT; Harris AL; Vaughan-Jones RD, Tumor-Associated Carbonic Anhydrase 9 Spatially Coordinates Intracellular pH in Three-Dimensional Multicellular Growths. Journal of Biological Chemistry 2008, 283 (29), 20473–20483. [PubMed: 18482982]

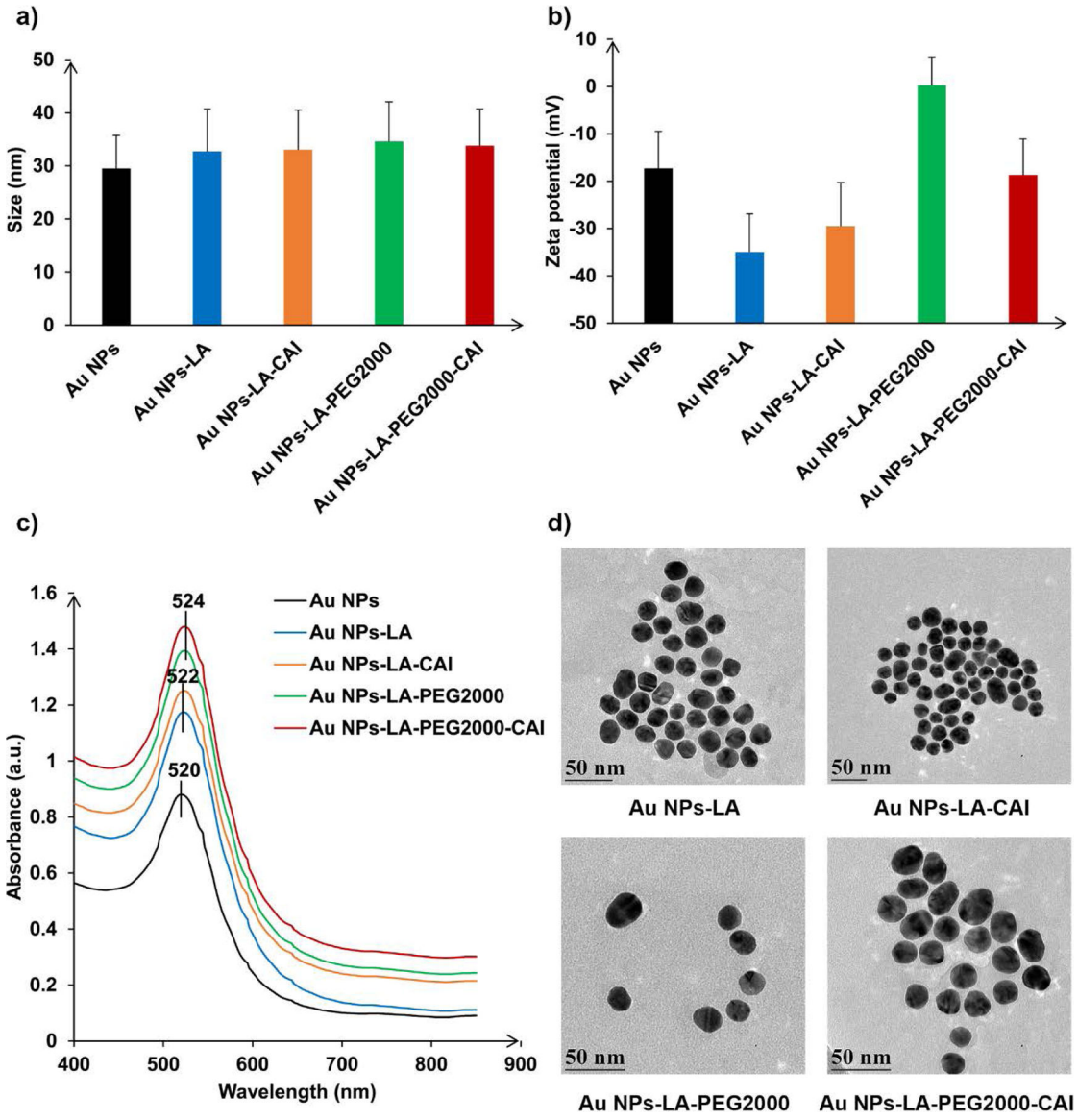

Figure 1.

Characterization of Au NPs functionalized with different ligands, revealing their a) size, b) zeta potential, c) plasmon spectrum and d) aspect (TEM image) and confirming the successful ligand exchange on Au surface.

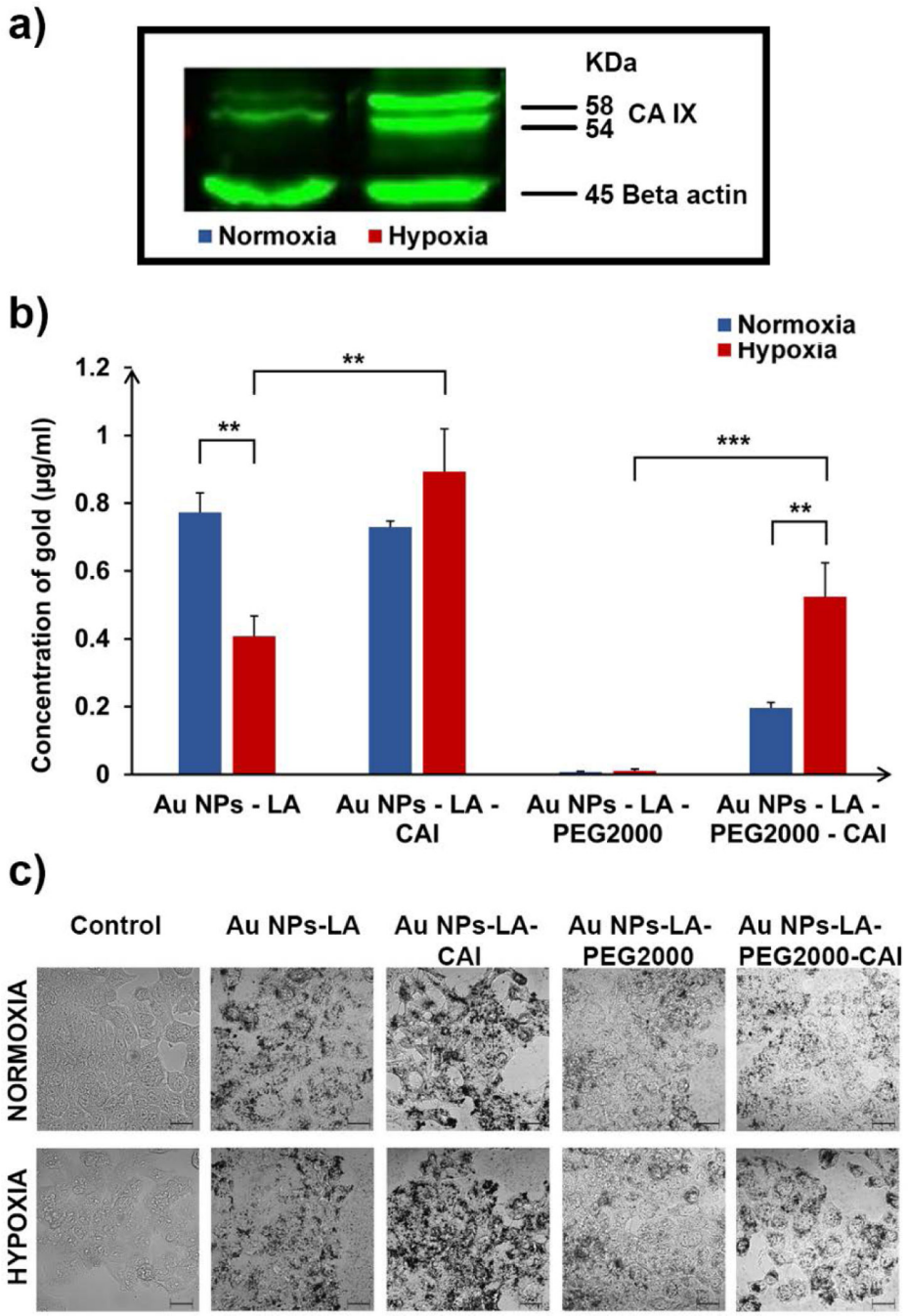

Figure 2.

Uptake of Au NPs bearing different surface ligands by HT-29 cells under normoxic and hypoxic condition depends on CA IX expression and on the Au surface ligands: a) CA IX expression in HT-29 cells under normoxic and hypoxic conditions, determined via western blotting; b) ICP-OES quantification and c) confocal microscopy post-silver staining for the uptake of ligand-functionalized Au NPs under both normoxic and hypoxic conditions (scale bar = 10 µm).

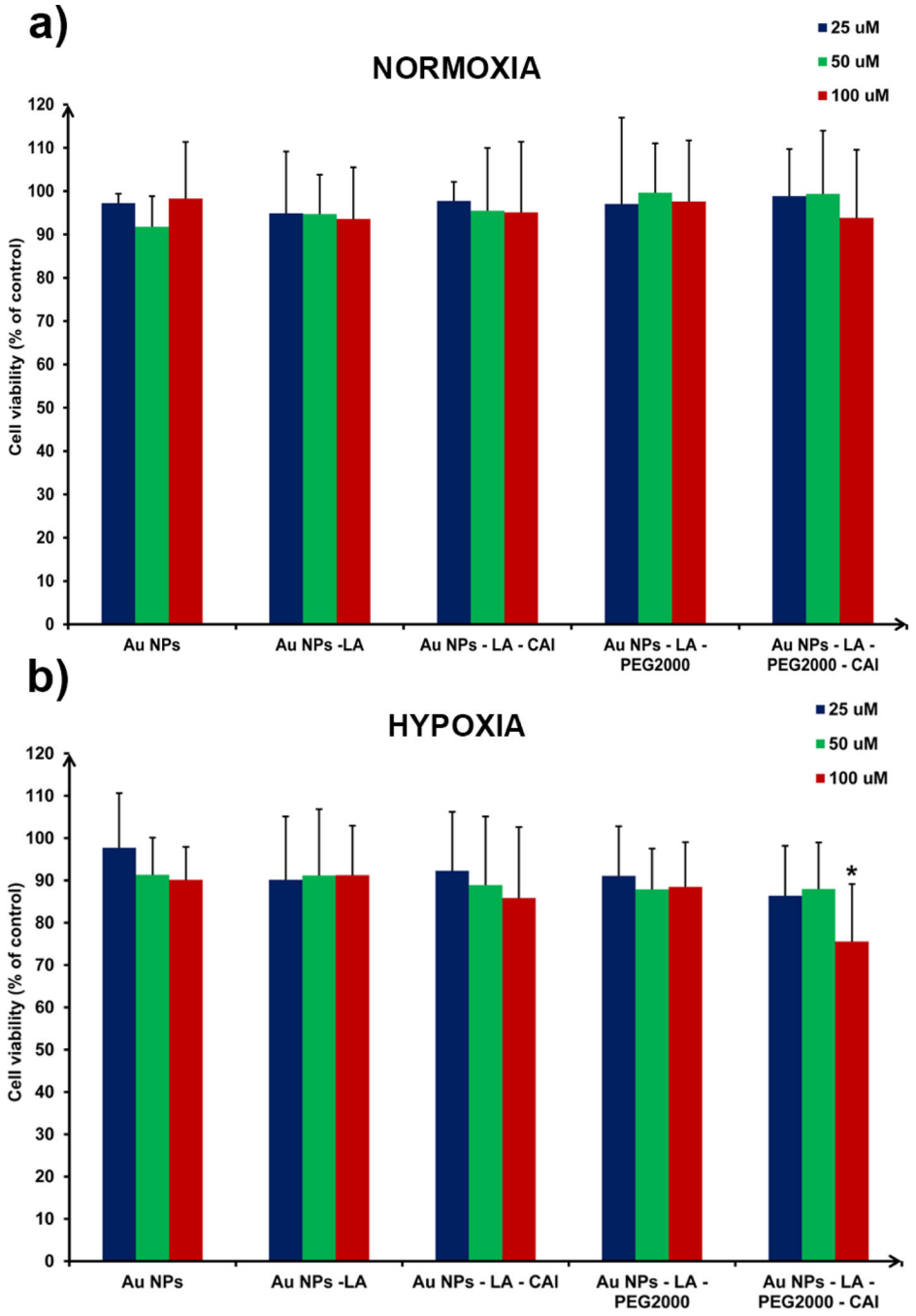

Figure 3.

Cell viability (by MTT assay) of HT-29 cancer cells treated with Au NPs bearing different surface ligands, at three different concentrations, under a) normoxic and b) hypoxic conditions. Au NPs-LA-PEG2000-CAI (100 μM) were able to kill cancer cells under hypoxic conditions in a statistically-significant manner ($P < 0.05$).

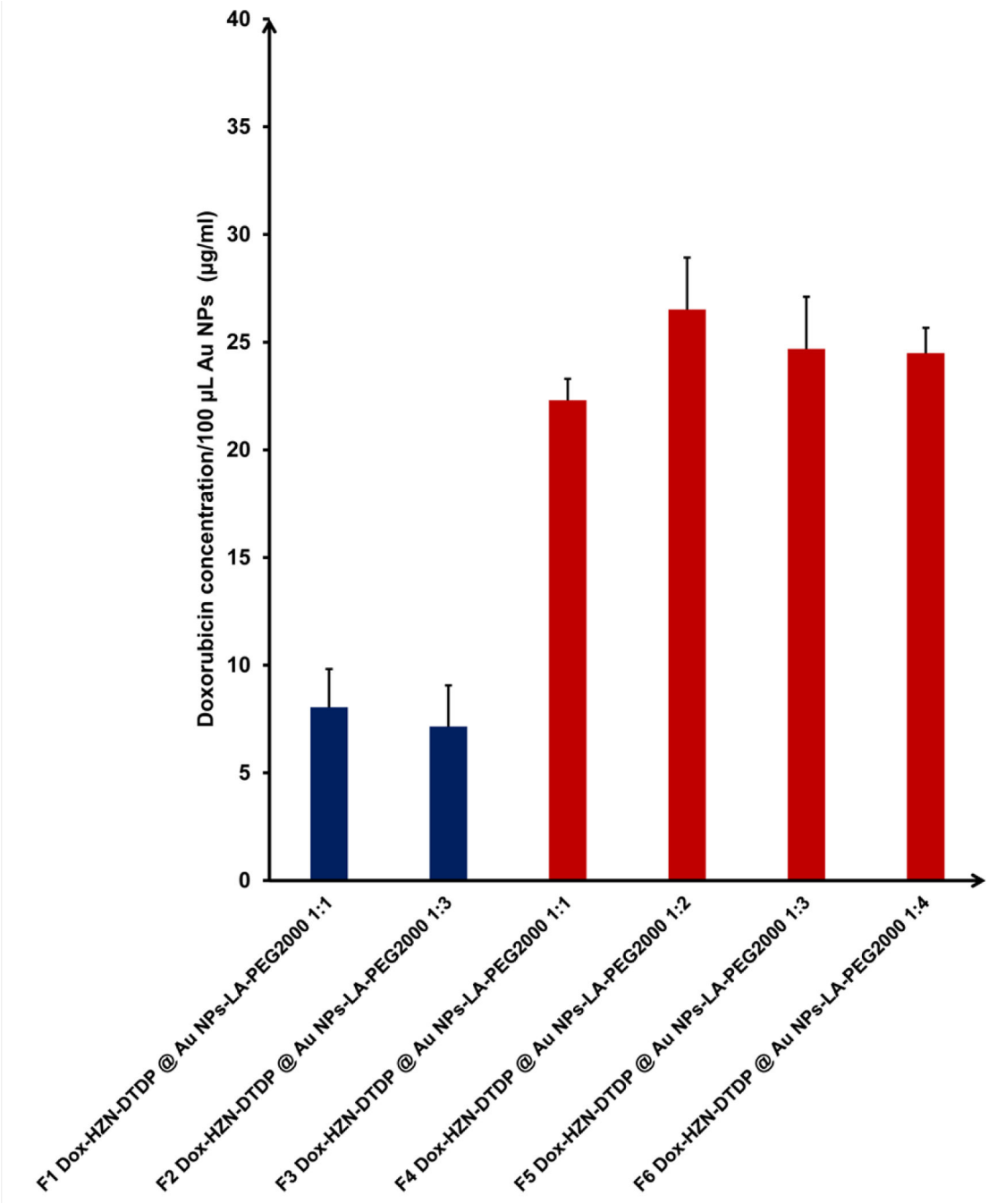

Figure 4.

Doxorubicin loading on PEGylated Au NPs using the DTDP-hydrazone linker strategy, emphasizing the drug loading outcome of different formulation strategies and conjugates used: on-bead Dox loading strategy (blue) versus pre-formed Dox-HZN-DTDP conjugate loading (red). The ratio of LA-PEG2000 to DTDP conjugate (mentioned in each case) did not affect the Dox loading outcome.

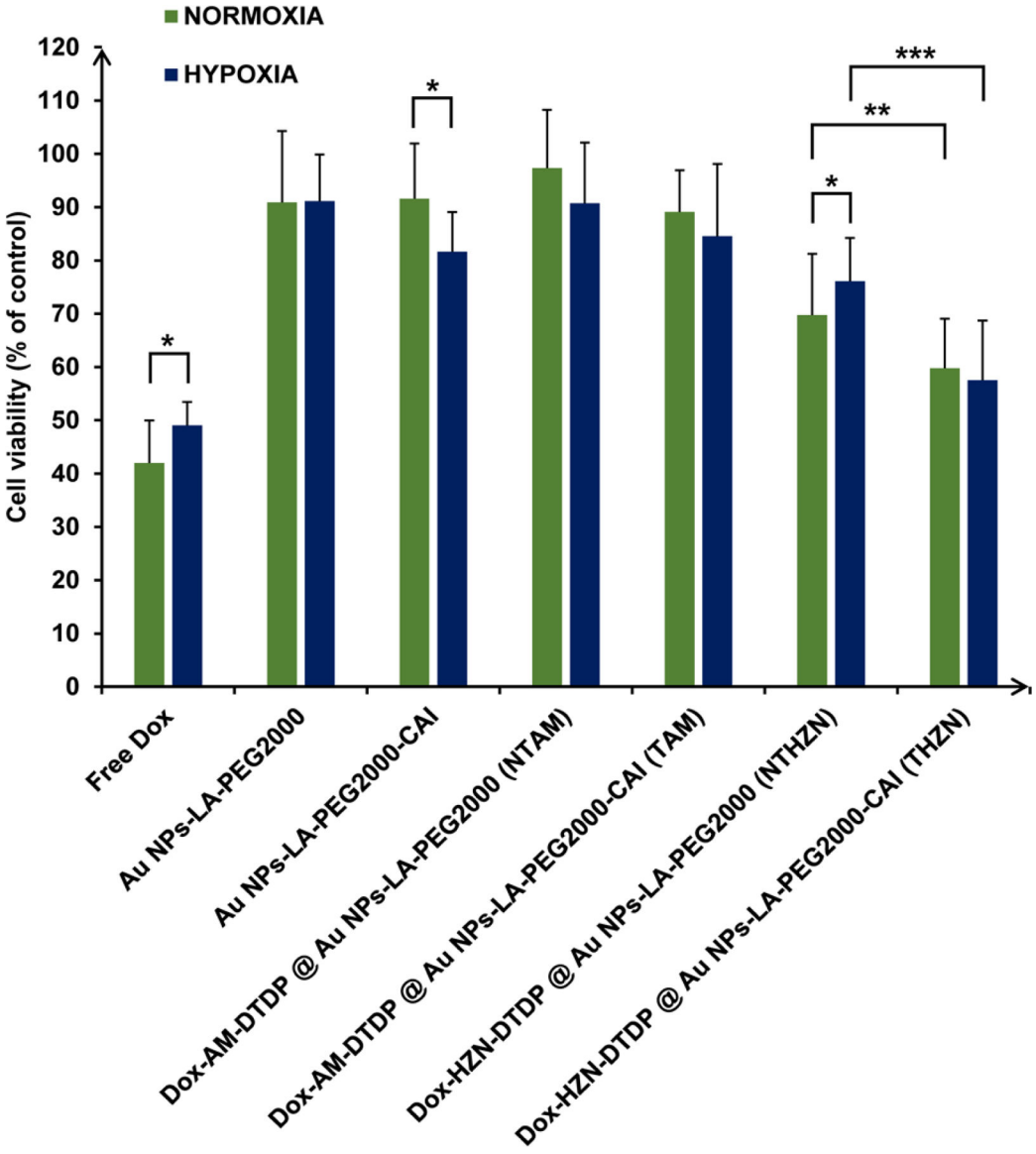

Figure 5.

Cytotoxicity assay (MTT) for HT-29 colon cancer cells post-treatment with free Dox, and with non-targeted (NT) and CA IX targeted- (T), unloaded and Dox-loaded Au NPs, bearing either amide (AM) or hydrazone (HZN) groups, under normoxic and hypoxic conditions. Note that CA IX targeted, HZN-bearing Au nanoplatform **THZN** enhanced the toxicity of doxorubicin under hypoxic conditions as compared with the non-targeted nanoplatform **NTHZN** ($P < 0.001$) and it also reversed the hypoxia-induced chemoresistance, observed for the free doxorubicin

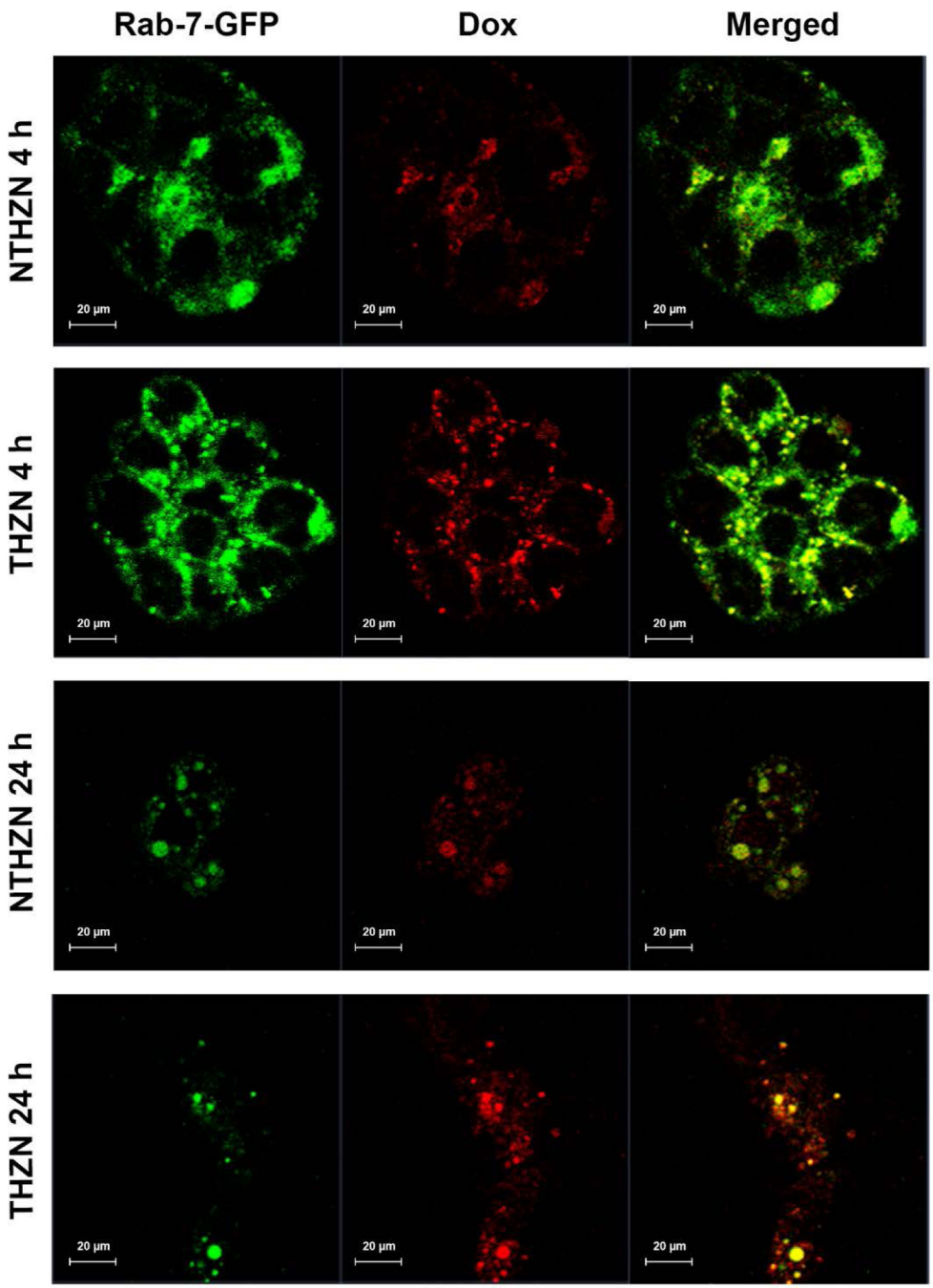

Figure 6.

Representative confocal microscopy images tracking the uptake of **NTHZN** and **THZN** nanoplatforms in HT-29 cancer cells transfected with the lysosomal marker Rab7-GFP, under hypoxic conditions, at either 4 h or 24 h incubation time. The comparative intracellular trafficking of the two Au nanoplatforms and the dynamic of doxorubicin release from them reflects the impact of CA IX-mediated internalization under hypoxic conditions.

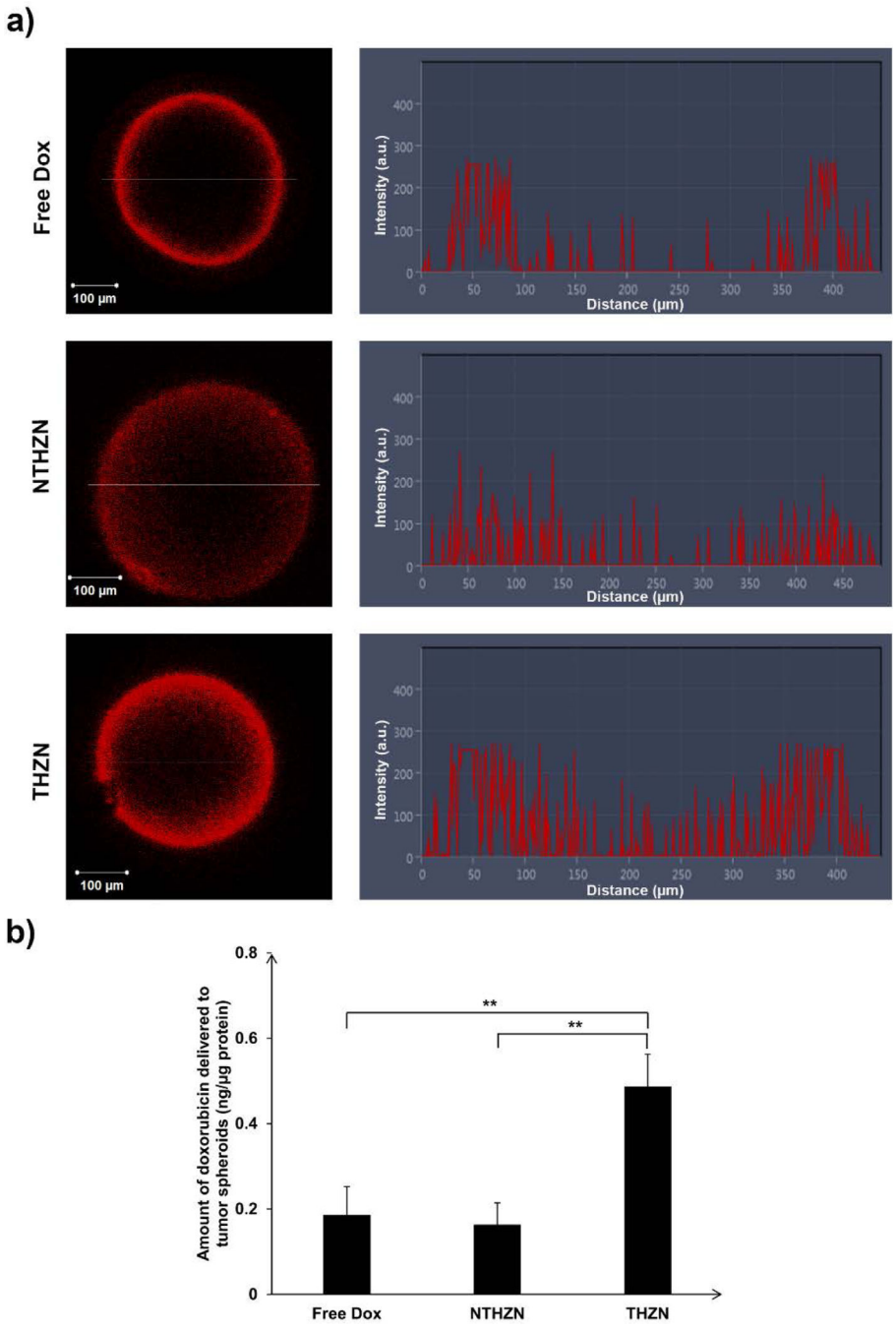

Figure 7.

Comparative delivery of doxorubicin into HT-29 tumor spheroids by **THZN**, **NTHZN** nanoplatforms versus free doxorubicin (at identical initial drug dose of 5 μg/mL), revealed via a) confocal fluorescence microscopy, showing spheroid image and fluorescence signal in cross section and b) quantified by fluorescence spectroscopy, post spheroid digestion.

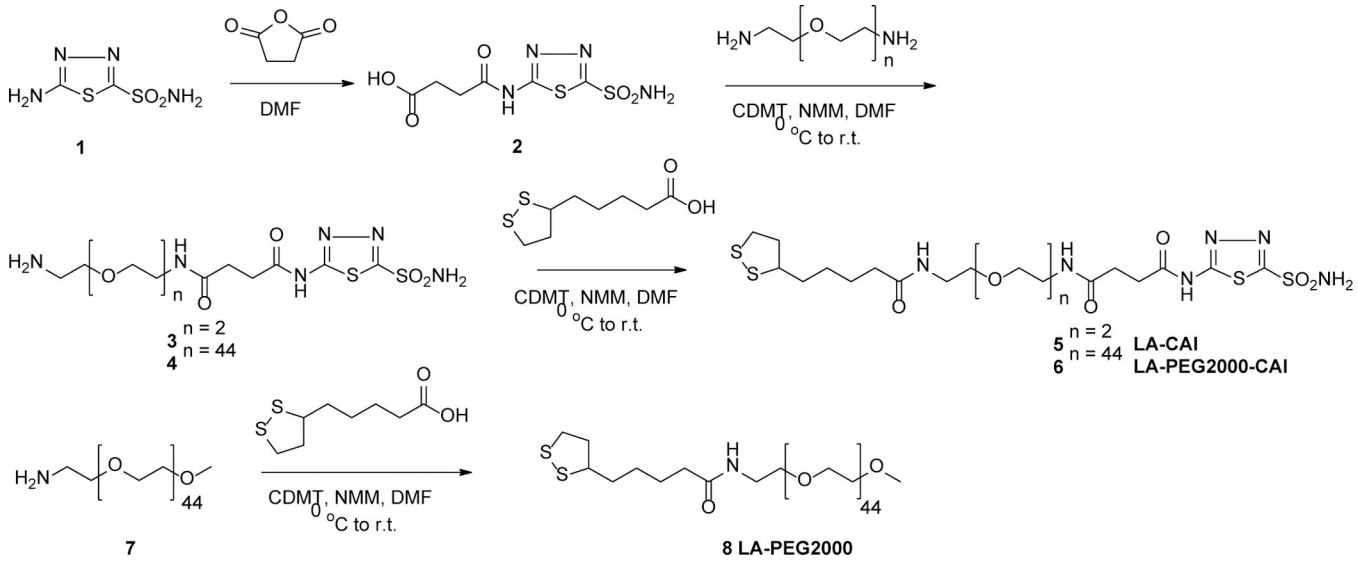

Scheme 1.

Synthesis of CA inhibitor targeting ligands **5** and **6**, bearing the 2-succinylamido-1,3,4,-thiadiazole-5-sulfonamide pharmacophore attached to lipoic acid anchoring moieties via either a short or long EG linker. An amino-PEG lipoic acid conjugate **8** (without the CAI pharmacophore) was also synthesized to be used in control experiments.

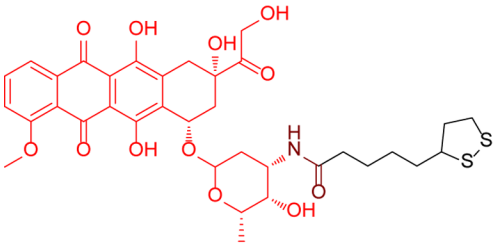

Dox-AM-LA

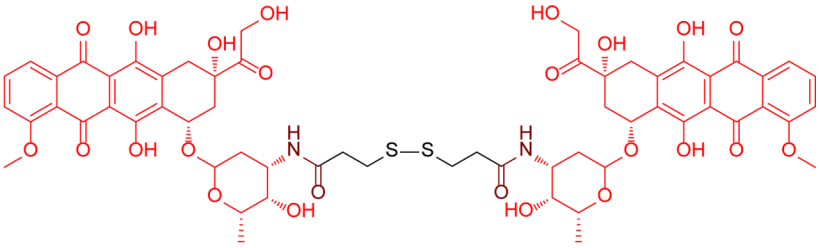

Dox-AM-DTDP

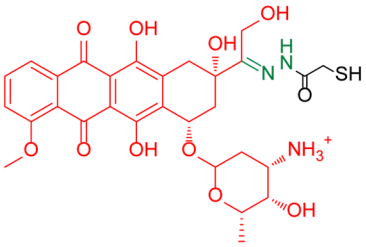

Dox-HZN-TG

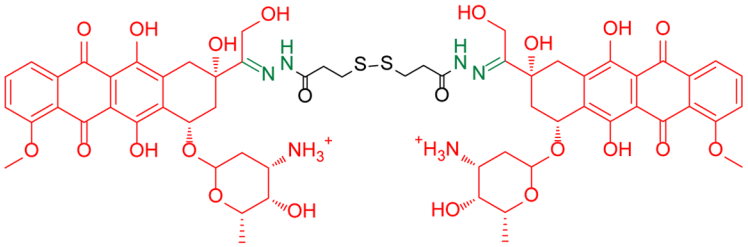

Dox-HZN-DTDP

Chart 1.

Structure of Dox conjugates used for doxorubicin loading onto the gold nanoplatform